Landslides
DOI 10.1007/s10346-020-01365-y
Received: 16 May 2019
Accepted: 28 January 2020

Corinne Singeisen · Susan Ivy-Ochs · Andrea Wolter · Olivia Steinemann · Naki Akçar · Serdar Yesilyurt · Christof Vockenhuber

The Kandersteg rock avalanche (Switzerland): integrated analysis of a late Holocene catastrophic event

Abstract In this study, we focus on the Kandersteg rock avalanche in the central Bernese Alps in Switzerland. We achieved an improved understanding of the release and emplacement of the rock avalanche through a combination of detailed field mapping, remote image analysis, reconstruction of deposit and source area volumes, and runout modelling with DAN3D. Based on cosmogenic ^{36}Cl dating of siliceous limestone boulders all across the landslide deposit, we determined an age of 3210 ± 220 years for the event. This age is markedly younger than the previously suggested age of 9600 years. An estimated 750–900 Mm^3 of Cretaceous limestones, siliceous limestones (Oehrlikalk, Kieselkalk and Bänderkalk formations) and Tertiary sandstones of the Doldenhorn nappe detached along pre-existing discontinuities from the northwest face of the Fisistock peak. The sliding body fragmented upon encountering the valley floor and the steep opposite valley wall. Next, the dry fragmented rock avalanche propagated northward over a substrate of fluvial sediments. As it moved, the debris became more fluid through entrainment of water and water-rich sediments, until it finally came to a halt 10 km downstream. The final volume of the deposit is estimated at 1.1 km^3. Our multi-method approach allowed us to establish that the deposit stems from one colossal event at 3.2 ka and to reconstruct the processes that dominated each phase of the rock avalanche. Our research contributes significantly to understanding not only the Kandersteg event but also complex emplacement processes and mechanics of large rock slope failures.

Keywords Landslide · Cosmogenic ^{36}Cl exposure dating · Runout modelling · Kandertal · European Alps

Introduction

Large slope failures constitute impressive features in mountainous landscapes and are part of the distinctive landscape of high-relief regions such as the Alps (Heim 1932; Abele 1974; Eisbacher and Clague 1984; Hewitt et al. 2008; Fort et al. 2009; Korup et al. 2010; Clague and Stead 2012). Although large-volume (> 10^6 m^3, Hermanns and Longva 2012) rock slope failures are infrequent, their often catastrophic effects pose a significant hazard to populations and infrastructure in mountainous areas. This is especially true when the mobility of the released material is increased significantly by transformation into debris flows as shown by the recent 2017 Piz Cengalo events in the Swiss Alps (Walter et al. 2020).

Rock mass strength, structure and topography are three of the major factors determining the stability of rock slopes (Gerber and Scheidegger 1969; Evans et al. 2006; McColl 2015; Stead and Wolter 2015). The strength of a material is mainly dependent on lithology and the condition and density of discontinuities, and it can be reduced through different processes such as weathering, tectonic activity, pore-pressure changes related to periods of heavy rainfall, permafrost degradation and large-amplitude freeze-thaw cycles (Schulz et al. 2009; Ravanel and Deline 2010; Krautblatter et al. 2013; Phillips et al. 2017). Discontinuities within a rock mass represent zones of weakness along which failure surfaces may develop. Stead and Wolter (2015) indicate that the tectonic damage present in slopes (fatigue) plays an important role when it comes to rock mass strength and the kinematics of rock slope failures. Finally, the topography of a site, including the presence of glacially or fluvially undercut and oversteepened slopes and dip slope configuration, determines if a slope is susceptible to large-scale instabilities (Agliardi et al. 2001; Brideau et al. 2009; Jaboyedoff et al. 2009; Hermanns et al. 2017). Perturbation of rock stress distribution and jointing, glacial erosion and debuttressing as well as ground shaking due to seismic events are discussed as possible preparatory and triggering factors (Evans et al. 2006; McColl et al. 2010; Leith et al. 2014; McColl 2015; Grämiger et al. 2017). In addition to highlighting causal factors and triggering mechanisms, much can be learned about emplacement dynamics by studying the landforms and sediments themselves in detail (McSaveney and Davies 2006; Crosta et al. 2007; Hewitt et al. 2008; Shugar and Clague 2011; Dunning and Armitage 2011; Weidinger et al. 2014; Dufresne et al. 2016; Wolter et al. 2016; Wang et al. 2018).

Covering an area of ~ 10 km² (Fig. 1), the Kandersteg deposits represent one of the largest catastrophic rock slope failures in the Alps (Abele 1974). Our study area encompasses the conspicuous failure scarp below the Fisistock peak (Fig. 2) and the extensive blocky deposits that fill the valley of Kandertal from just south of the village Kandersteg to 9 km downstream (Bachmann 1870; Brückner 1897; Fellenberg et al. 1901; Turnau 1906; Heim 1932; Nussbaum 1934; Furrer et al. 1993; Tinner et al. 2005). The deposits were first mapped as glacial sediments and the numerous transverse ridges interpreted as moraines (Bachmann 1870). At a road construction site in 1891, Brückner (1897) immediately recognized the poorly sorted sediment with little lithological variation of the very angular clasts as a huge landslide deposit. Similarly, Turnau (1906), Heim (1932) and Nussbaum (1934) interpreted the deposits as resulting from a single landslide event from the obvious niche on the NW face of Fisistock. In contrast, Beck (1929) distinguished two independent events: an older event represented by fine-grained, porous, whitish sediment underlying a younger megablock deposit. Beck (1952) proposed that the lower deposit was the result of a rock avalanche from the peak known as Bire (Fig. 1) and the overlying boulder-dominated deposit formed through multiple events from the Fisistock area. Turnau (1906), on the other hand, interpreted the fine material underlying the boulder-rich surface deposit as the product of comminution during landsliding in a single event originating from Fisistock. He estimated a volume of 900 Mm^3 and calculated a Fahrböschung angle of 10–11° (H_{max}/L_{max} = 0.19). The lack of boulders in the Kandersteg basin between the deposits at Schattwald and the town of Kandersteg led Fellenberg et al. (1901) to suggest that the rock avalanche fell onto a glacier. Conversely, Turnau (1906) concluded that the event could only have occurred post glacially as

Published online: 08 February 2020

local residents reported the finding of tree trunks in the landslide deposits. Based on ^{14}C dating of sediments near Frutigen (Fig. 1), Tinner et al. (2005) estimated that a rock avalanche, which they correlated to the younger event suggested by Beck (1929, 1952), occurred 9600 years ago with a lake impounded in the Kandersteg area. They hypothesized that the landslide dam breached 200–500 years later and there was a catastrophic outburst flood.

Despite numerous studies, no consensus regarding the failure and emplacement processes of the event(s) has yet been found. It is thus the intent of the present work to shed light on open questions regarding the timing, failure and movement dynamics of the Kandersteg rock avalanche. Based on detailed field analysis of landforms and sediment in both the release and deposition area, combined with remote image interpretation, DAN3D runout modelling and cosmogenic nuclide dating, we reconstruct detachment and emplacement of the rock mass released from the Fisistock northwest slope.

Setting

The study area is located in the Bernese Alps of central Switzerland in the catchment of the Kander River. Kandertal is a broad valley bound by steep valley walls and surrounded by high mountain peaks. The most prominent peaks are Doldenhorn (3638 m a.s.l.), Innere and Üssere Fisistock (2787 and 2947 m a.s.l.) and Bire (2502 m a.s.l.).

During the Last Glacial Maximum (24 ka; Ivy-Ochs 2015), a huge valley glacier filled Kandertal up to an elevation of 1800–1900 m a.s.l. (Bini et al. 2009). By 18 ka, the forelands and likely Kandertal were free of ice. Re-advance of local glaciers into Kandertal during the Gschnitz stadial (17–16 ka) and Egesen stadial (13–12 ka) is presumed but undated in this region. Locating the Lateglacial ice fronts is difficult in Kandertal as the valley is filled with at least 400 m of Lateglacial and Holocene sediments (Kellerhals and Isler 1998).

The Kandersteg rock avalanche source area is located in the Helvetic nappes (Fig. 1). The main units in the area are the para-autochthonous Doldenhorn nappe (separated from the Aar massif by a major Alpine thrust fault) and the allochthonous Gellihorn, Drusberg and Wildhorn nappes (Zwahlen 1986; Furrer et al. 1993; Kellerhals and Isler 1998; Pfiffner 2010). The upper part of Fisistock comprises sedimentary rocks belonging to the Doldenhorn nappe ranging in age from Malm to Tertiary. The landslide source area (Fig. 2) includes Oehrlikalk limestone underlain by and at the base interbedded with Oehrlimergel marl layers. These limestones are overlain by Kieselkalk (siliceous limestone) and Bänderkalk with Numulitensandstein and Lithothamnienkalk followed by Globigerinenschiefer (shale) on top (Adrian 1915; Krebs 1925; Furrer et al. 1993; Pfiffner 2010). There is one large fold in the Fisistock release area, the recumbent Doldenhorn fold, whose upper limb is exposed on the northwest side of Fisistock (Pfiffner 2010). Its fold axis is oriented NE–SW. Regional normal faults are oriented NNW–SSE, and thrust faults separate the nappes (Zwahlen 1986; Kellerhals and Isler 1998; Pfiffner 2010).

The Bire (Fig. 1) is formed by rocks belonging to both the Gellihorn and the Wildhorn nappes. Exposed rocks from bottom to top are Flysch (Tertiary), separated by a tectonic contact from Oehrlimergel, Oerhlikalk and Taveyannaz sandstone (Gellihorn nappe), which are separated by a tectonic contact from the overlying Birmensdorf formation and Malmkalk (Wildhorn nappe) (Furrer et al. 1993; Pfiffner 2010).

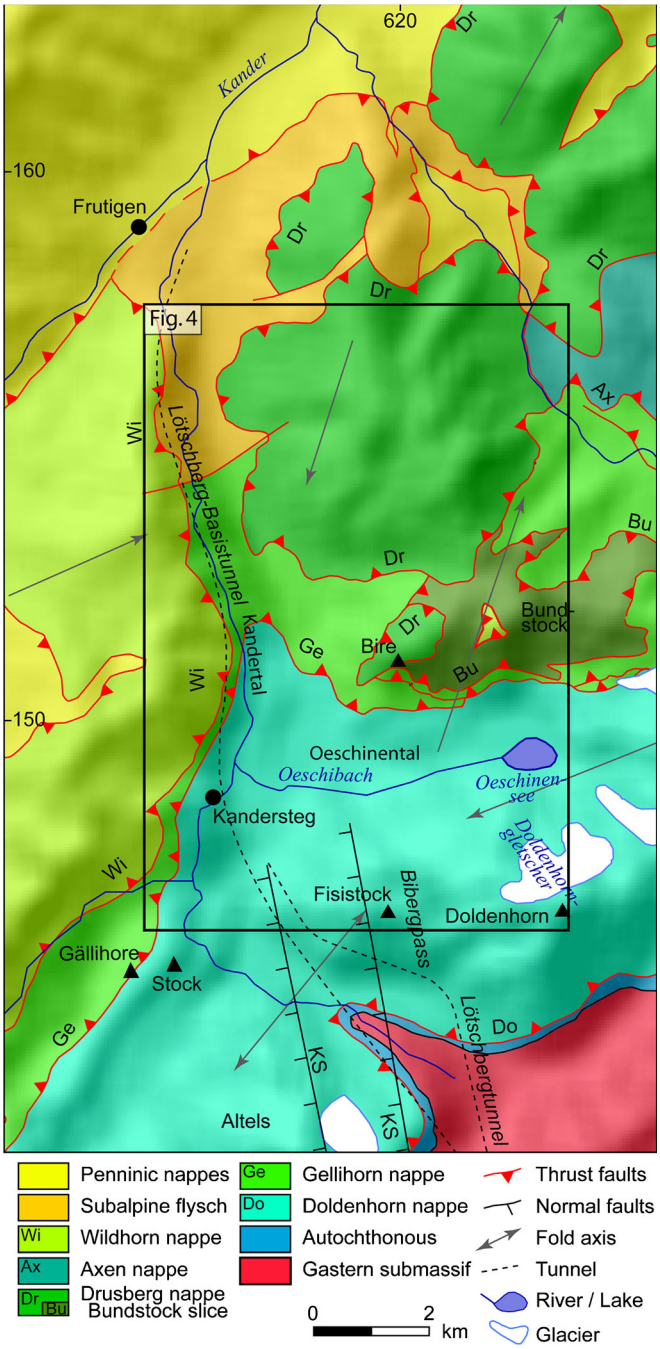

Fig. 1 Tectonic sketch map of the main tectonic units and faults in the Kandertal region (modified from Pfiffner 2010). Wildhorn, Axen, Drusberg, Gellihorn, Doldenhorn nappes all belong to the Helvetic nappes. KS indicates Kandertal Störung (Zwahlen 1986). Study area (Fig. 4) indicated by black square. Extent of Kandersteg rock avalanche deposits and source area just north of Fisistock are shown in Fig. 4

Methods

Fieldwork and remote image interpretation

We combined detailed geomorphological field mapping, outcrop description, interpretation of aerial images and a 0.5-m LiDAR

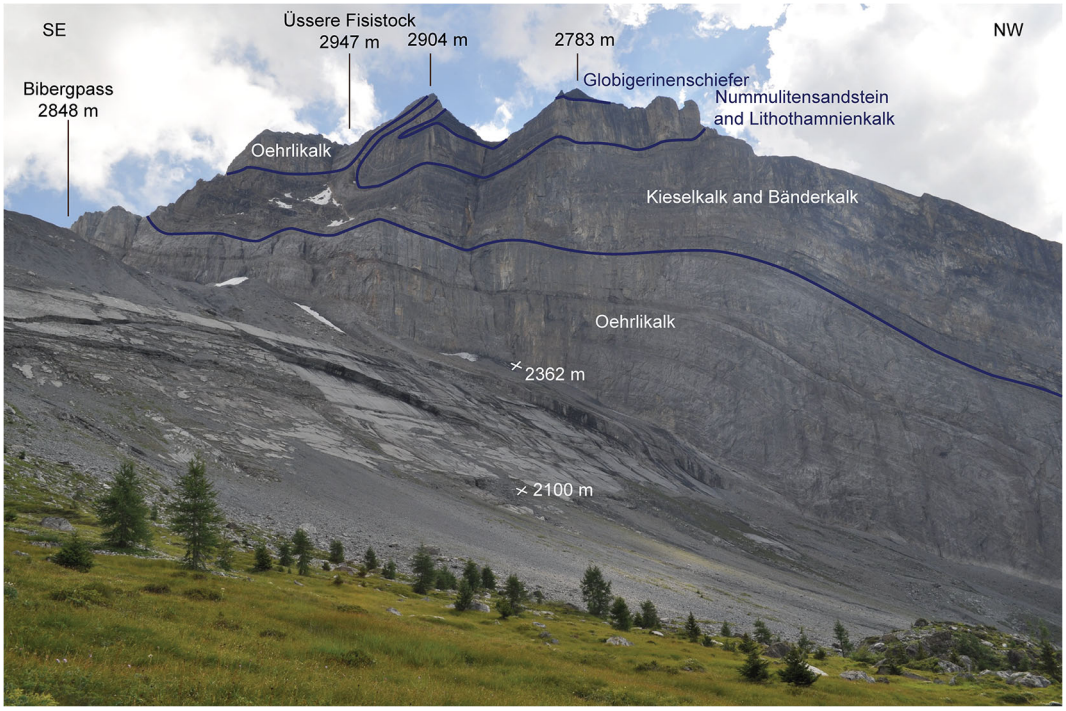

Fig. 2 Photo of Fisistock niche source area of the Kandersteg rock avalanche and outcropping Cretaceous and Eocene units of the Doldenhorn nappe (after Furrer et al. 1993). View is to the south, movement direction was to the right and towards the observer (photo: C. Singeisen, September 2016)

digital elevation model (DEM), as well as construction of cross-sections, to understand the origin and timing of the deposits in Kandertal. The regional orientation of bedrock faults and structures was identified through lineament mapping on the DEM. We characterized the sedimentology of the landslide debris based on outcrop descriptions. Extensive fieldwork was required to map the distribution and lithologies of the boulders present. Thin section analysis was also used to correlate boulder lithologies with bedrock exposed in the source area based on mineralogy and fossils present. A total of 259 structural measurements were taken at outcrops in the study area. Joint sets were defined based on a stereographic representation of the joint measurements using the RocScience software Dips. Joint persistence and spacing were qualitatively described according to ISRM (1978).

^{36}Cl exposure dating

Eleven samples were collected for surface exposure dating with cosmogenic ^{36}Cl. Nine are from siliceous limestone boulders in the deposits (Kieselkalk, Bänderkalk) and two are from Oehrlikalk bedding planes in the source area bedrock. The tops of large boulders (Fig. 3) located in topographically high positions with respect to the surroundings were selected.

Rock samples were prepared following the method of isotope dilution (^{35}Cl) described in Ivy-Ochs et al. (2004). Total Cl and ^{36}Cl were measured in the same target at the ETH accelerator mass spectrometry (AMS) facility of the Laboratory for Ion Beam Physics (LIP) with the 6 MV tandem. Measured ^{36}Cl/Cl ratios were normalized to the ETH internal standard K382/4N with a value of $^{36}\mathrm{Cl/Cl} = 17.36 \times 10^{-12}$, which is calibrated against the primary ^{36}Cl standard KNSTD5000 (Vockenhuber et al. 2019). A full process chemistry blank (3.2×10^{-15}) was subtracted from measured sample ratios. This amounted to a correction of 3% or less for all samples. All eleven samples were prepared for AMS measurement, with nine exposure ages obtained (Table 1). For Kander 3 and Kander 9, AMS measurement was stopped because of high ^{36}S interferences.

To calculate ^{36}Cl exposure ages we used the LIP ETH in-house MATLAB code based on the parameters presented in Alfimov and Ivy-Ochs (2009 and references therein). This includes production from all pathways as well as non-cosmogenic production based on the measured elemental composition of every rock sample (Table 2). The production rates used are in excellent agreement with ^{36}Cl production rates recently published by Marrero et al. (2016). Exposure ages were corrected for karst dissolution using a rate of 0.5 cm/ka. Final errors on the ages (Table 1, Fig. 4) include both analytical and production rate uncertainties.

Volume estimation and runout modelling

An approximate volume of the landslide deposits could be derived from field data as well as from borehole logs and seismic data given in the Lötschberg tunnel publications (Kellerhals and Isler 1998; Ziegler and Isler 2013). The 35 borehole logs from drill cores taken in the area (Geoportal Kanton Bern, www.map.apps.be.ch) were evaluated. Nevertheless, in the Kandersteg area only cores 91/1 and 91/5 (locations shown on Fig. 4) reached below the landslide deposits.

Pre-event topography in the source area was created using the software RHINOCEROS v. 5, based on present-day geomorphology as well as mapped and interpreted bedrock structures (Kellerhals and Isler 1998). Before computing the volume of the release area, the debris (mostly talus) present today in the release area was removed in GIS through interpolation of contour lines. Pre-failure

Fig. 3 Photos of several ^{36}Cl-dated boulders in the Kandersteg deposits. Boulder heights listed in Table 1. DH1 is a bedrock sample in the release area (location shown on Fig. 4)

contours in the deposition area were drawn, converted into points and added to the point-cloud of the DEM in ArcGIS. The raster surface of the pre-failure topography was then reconstructed using the natural neighbour tool in ArcGIS. Volumes were calculated in ArcGIS using the Cut/Fill tool.

We simulated the dynamics of the Kandersteg rock avalanche using DAN3D, a runout code applying the Lagrangian numerical method to model granular flows as equivalent fluids (Hungr 1995; McDougall and Hungr 2004; Hungr and Mcougall 2009). Input parameters required to simulate runout include path topography, source volume and rheological parameters. We applied the most likely volume scenario (750 Mm^3), which includes the Schattwald deposits in the Kandersteg event. Simulations excluding the Schattwald deposits were not run, as this decreased deposit volume was considered to be too small compared with the estimated source volume. We hypothesize a pre-event landscape comprising a glacially formed, steep-walled U-shaped valley covered with several hundred meters of saturated alluvial sediment interbedded with glacial sediments in the lower part (cf. Kellerhals and Isler 1998). For the input path topography, we used a flat, gently northward sloping valley floor with steep valley walls as suggested by geophysical data. This was kept the same for all model runs.

The rheological parameters in DAN3D are determined through calibration and back-analysis and include internal friction of the materials and basal friction parameters. Most parameters, such as the unit weight, stiffness coefficient and smoothing length coefficient, were kept at the default values. Several authors, such as McDougall (2006) and Hungr and Mcougall (2009), demonstrate that these parameters do not affect model results significantly. Hungr (1995) and Aaron and Hungr (2016) show that the

Table 1 Site information and AMS data for samples from Kandersteg rock avalanche boulders and release area bedrock (DH 1, DH 2)

Sample	Boulder height (m)	Lat (°N)	Long (°E)	Elevation (m a.s.l.)	Thickness (cm)	Shielding	Cl (ppm)	^{36}Cl (10^5 atoms g_{rock}^{-1})	Exposure age (years)
Kander 1	2.4	46.5012	7.6687	1313	4	0.972	7.78 ± 0.05	1.355 ± 0.074	3300 ± 210
Kander 2	2.2	46.5012	7.6686	1313	3	0.971	5.52 ± 0.02	1.712 ± 0.082	3280 ± 190
Kander 3	3.5	46.5019	7.6690	1311	2	0.967	n.d.	n.d.	
Kander 4	1.7	46.5038	7.6667	1328	3	0.953	5.33 ± 0.02	0.790 ± 0.069	3000 ± 280
Kander 5	1.6	46.5021	7.6657	1332	3	0.959	3.87 ± 0.01	1.170 ± 0.064	2980 ± 190
Kander 6	1.8	46.5034	7.6671	1332	4	0.964	4.40 ± 0.02	1.565 ± 0.093	4330 ± 290
Kander 7	3.6	46.5331	7.6687	921	3	0.942	6.31 ± 0.04	0.967 ± 0.147	3550 ± 550
Kander 8	3.2	46.5331	7.6692	928	3	0.941	4.76 ± 0.02	1.023 ± 0.059	3130 ± 210
Kander 9	5	46.5342	7.6683	916	3	0.935	n.d.	n.d.	
DH 1	bedrock	46.4847	7.7067	2134	2.5	0.953	15.91 ± 0.08	1.750 ± 0.089	1710 ± 100
DH 2	bedrock	46.4844	7.7065	2144	3	0.956	15.09 ± 0.07	2.010 ± 0.099	1940 ± 120

All mechanisms for production of ^{36}Cl are included, production rates and constants given in Ivy-Ochs et al. (2009). Production rate of ^{36}Cl from spallation of Ca is 54.0 ± 3.5 ^{36}Cl atoms g_{Ca}^{-1} $year^{-1}$, with 9.6% muon contribution at the surface (Stone et al. 1996). For low-energy neutron capture production, a value of 760 ± 150 neutrons g_{air}^{-1} $year^{-1}$ was implemented

Table 2 Elemental data for samples from Kandersteg rock avalanche

Sample	SiO_2 wt%	Al_2O_3 wt%	Fe_2O_3 wt%	MnO wt%	MgO wt%	CaO wt%	Na_2O wt%	K_2O wt%	TiO_2 wt%	P_2O_2 wt%	Sm ppm	Gd ppm	U ppm	Th ppm
Kander 1	28.17	1.36	2.78	0.02	0.55	35.58	0.08	0.62	0.07	0.09	2.5	2.1	0.9	4.0
Kander 2	10.82	0.54	1.33	0.02	0.21	47.93	0.04	0.28	0.02	0.07	1.9	1.9	0.9	1.5
Kander 3	28.04	0.94	1.93	0.03	1.02	36.21	0.04	0.52	0.06	0.07	2.1	1.8	1.6	2.7
Kander 4	55.68	1.89	2.21	0.03	0.45	21.68	0.04	0.72	0.11	0.09	3.2	2.8	1.8	3.2
Kander 5	32.01	1.04	0.87	0.02	0.29	35.94	0.11	0.37	0.07	0.05	1.3	1.1	1.0	1.7
Kander 6	36.41	1.55	1.48	0.02	0.37	31.71	0.15	0.60	0.10	0.06	1.8	1.5	1.0	2.7
Kander 7	35.19	1.30	3.17	0.03	0.57	32.85	0.03	0.76	0.09	0.12	2.6	2.3	1.4	4.2
Kander 8	21.86	0.78	1.49	0.04	0.34	41.28	0.05	0.40	0.05	0.07	1.7	1.5	1.9	2.3
Kander 9	18.98	1.17	2.17	0.03	0.47	42.51	0.10	0.59	0.05	0.08	2.1	1.8	1.0	3.0
DH 1	2.96	1.56	0.66	0.01	0.80	50.79	0.04	0.45	0.07	0.05	0.6	0.5	1.4	0.9
DH 2	2.07	1.14	0.51	0.01	0.78	51.98	0.05	0.32	0.05	0.04	0.4	0.4	1.1	0.7

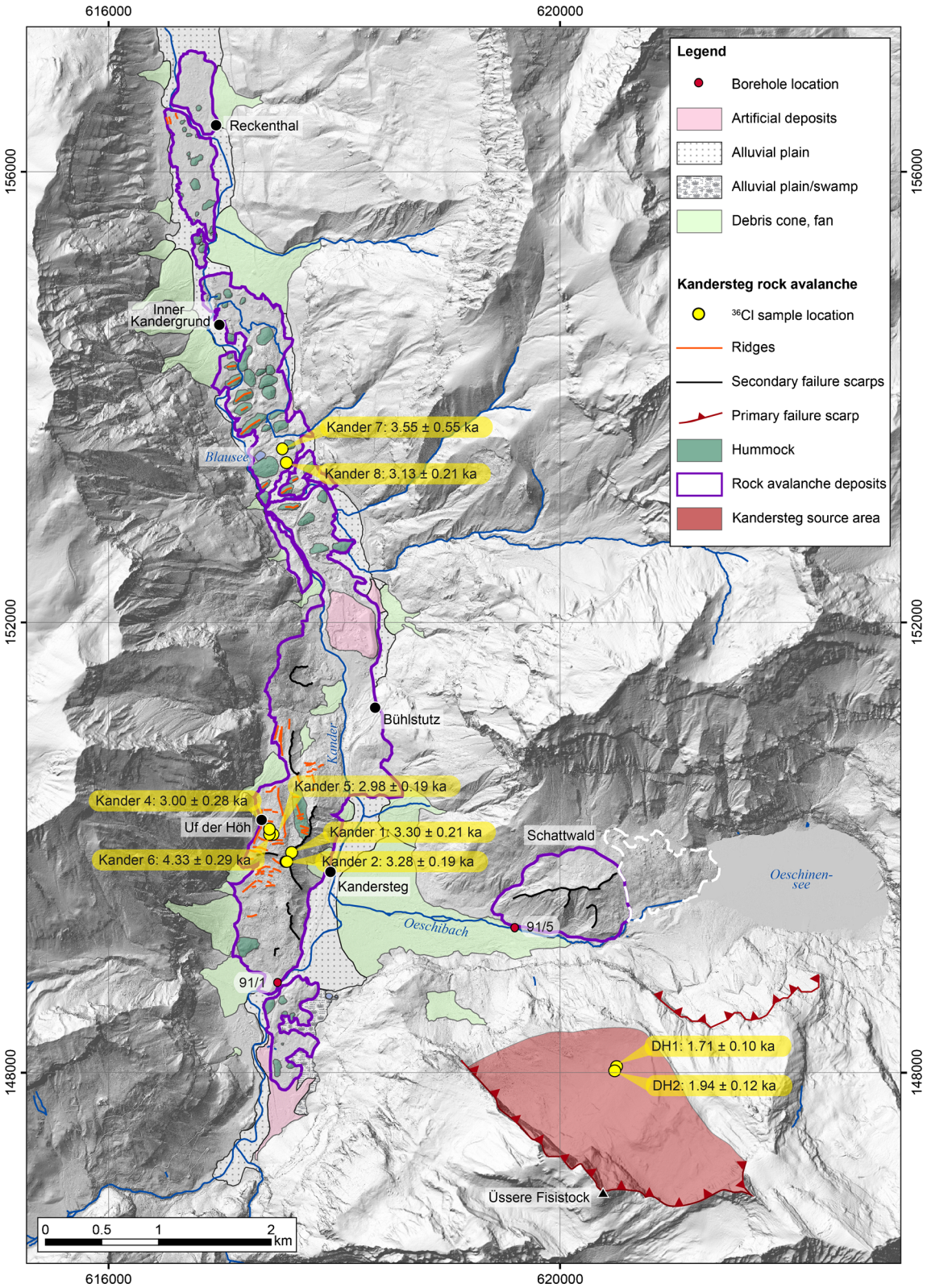

Fig. 4 Geomorphological map of the Kandersteg rock avalanche. All obtained ^{36}Cl exposure ages from boulders and basal release plane are shown (Table 1). Red points indicate locations of cores discussed in the text. White dashed line shows extent of Oeschinensee rock avalanche deposits, release area scarp is located just to the south (based on Köpfli et al. 2018)

internal friction angle controls spreading and run-up behaviour, but that results are insensitive to this parameter so long as it is kept within a reasonable range (25 to 35°). We kept the internal friction angle constant at 35°. We conducted sensitivity analyses on rheological model and basal friction parameters, completing more than 80 simulations (see Supplemental Material). First, the frictional and Voellmy rheological models, both commonly used in rock avalanche simulation, were compared, and it was determined that the Voellmy rheological model resulted in more realistic runout extent and velocities. In particular, the frictional rheology produced numerical instabilities for the Kandersteg simulations. Next, the effect of multiple substrate materials was analysed. First-order sensitivity analysis was carried out with homogeneous material properties throughout the model to obtain the most reasonable range of material properties. In a next step these results were compared with two- and three-material models, with different properties for the bedrock sliding plane in the source area, valley floor alluvial sediments and surrounding material. For these three different material scenarios, we calibrated the Voellmy basal friction and turbulence coefficients. Körner (1976) and Aaron et al. (2019) showed that, for a given runout extent, the friction and turbulence coefficients are not unique. We therefore expect that multiple combinations of friction and turbulence parameter would reproduce the same runout extent ('parameter non-uniqueness'). Since our goal was to confirm our hypothesized single failure scenario, exploring the parameter non-uniqueness was not considered necessary. If this event is used as a precedent for prediction, parameter non-uniqueness should be explored.

The best-fit model was determined to be a Voellmy model with three materials. Finally, the best-fit scenario was analysed for the effect of bulking or erosion and entrainment of material. Three further simulations were run: (i) no bulking, (ii) bulking (25%, Hungr and Evans 2004) and (iii) bulking and entrainment of path material, using the erosion rate calculator tool in DAN3D. Erosion rates were specified using an erosion path of 2 km and the initial and final slide volumes. The value determined with the erosion rate calculator tool in DAN3D was then used to model the runout and obtain a final volume. For the no bulking/no erosion entrainment model, the volume was that of the source area, 750 Mm^3. With inclusion of 25% bulking (DAN3D erosion rate of 0.00011 m s^{-1}), a volume of 950 Mm^3 (1.25 × 750 Mm^3) was determined. When both erosion and entrainment of valley floor sediments (erosion rate of 0.00019 m s^{-1}) were included, a volume of 1130 Mm^3 was obtained. Results of the runout modelling include information on the travel path, movement, velocity gradient and final deposit thickness and extent.

The Kandersteg rock avalanche: geomorphology and age

Release area assessment and structural measurements

The release area on the northwest slope of Fisistock is a 2.2-km-long, 800–1200-m-wide distinctly box-shaped niche (Fig. 2). Displaced rock comprises mainly Oehrlikalk, Kieselkalk and Bänderkalk formations. The back scarp is about 100 m high including the low at Bibergpass (Fig. 1), while the prominent steep western sidewall is 350–500 m high. The eastern lateral boundary is difficult to constrain.

During field mapping, four joint sets were recognized (Fig. 5c). Joint set So (mean 165/10, $n = 53$) is parallel to bedding and is oriented sub-horizontally, with spacing ranging from about 10 cm to 2 m, depending on bedding thickness. Persistence (ISRM 1978) of So varies between several centimetres and a few

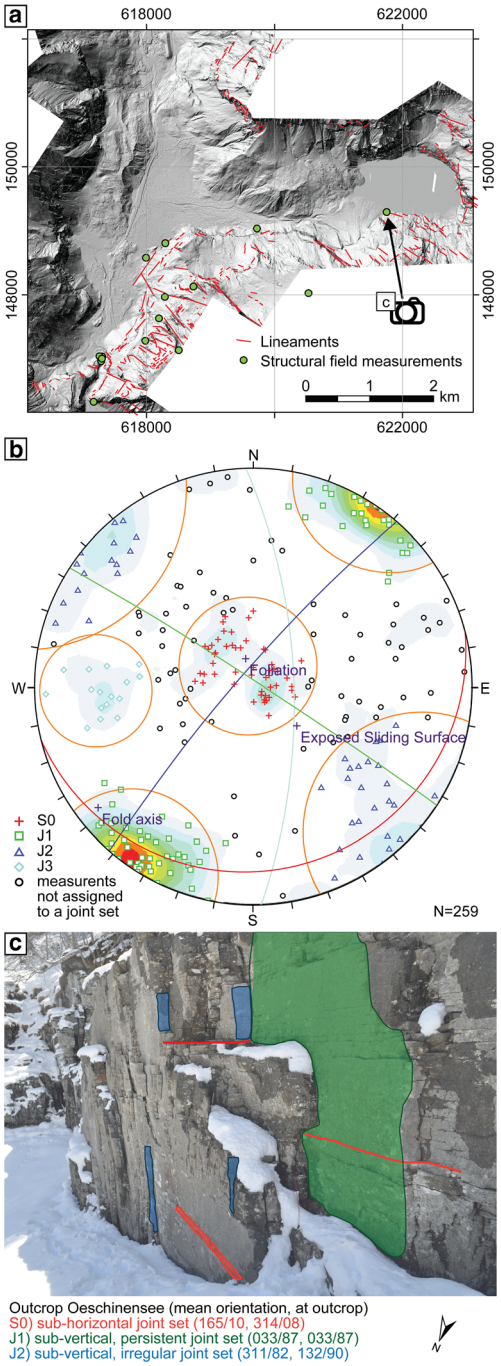

Fig. 5 **a** Mapped lineaments and locations of structural measurements taken in the field (green points). Location of photo of c shown. **b** Stereoplot of joint measurements taken in the field. Contours range from 0 to 12%, intervals are 1.2% as defined with Fisher distribution (Fisher 1953); orange circles represent 2STDEV variability cones. **c** Outcrop photo (location 621751/149292), joint set J1 (green) is persistent, whereas joint set J2 (blue) is irregular; set S0 (red lines) is sub-horizontal and is oriented parallel to bedding. (621751/149292). Height of wall is 2 m (photo: C. Singeisen 2017)

meters. The dip angle of the bedding varies between 35° and 10°, with the shallower dip occurring where the bedding planes daylight in the steep rock cliffs at the base of the release area. The slope angle of the basal failure surface predominantly follows bedding planes (S0) (Fig. 6b). ^{36}Cl exposure ages were determined (Table 1) for two samples from the basal plane bedrock, with ages of 1.71 ± 0.10 ka (DH 1) and 1.94 ± 0.12 ka (DH 2).

Three vertical to sub-vertical joint sets (J1, J2, J3) were mapped in the field (Figs. 5 and 6). Joint set J1 (mean 033/87, $n = 76$), striking NW–SE and dipping sub-vertically, can be identified in most outcrops in the study area. Persistence and spacing reach several meters in some outcrops. In the field, the rock wall of the SW flank is characterized by extremely closely spaced J1 joints (ca. 5 cm). This suggests that the lateral scarp follows a pre-existing fault structure that facilitated detachment. This hypothesis is supported by analysis of thin sections. Samples of Oehrlikalk taken at the lateral release scarp show tectonic overprinting and deformation of ooids in thin section. In contrast, thin sections from bedrock away from this fault do not show deformation. Joint set J2 (mean 311/82, $n = 43$) is oriented NE–SW and dips sub-vertically to the NW. Persistence and spacing vary from decimetres to meters in scale. The head scarp in part follows these steeply NW dipping discontinuities (J2). Joint set J3 (088/69, $n = 17$) is a minor joint set steeply dipping towards the east and is only defined by 17 measurements. This joint set is mainly observed along the north-facing wall of the Fisistock massif just above Oeschibach (location shown in Fig. 5a).

Based on analysis of the DEM, two main orientations of lineaments were identified (Fig. 5a). In the lineament analysis, only steep discontinuity sets could be identified. One is oriented NW–SE (mean strike direction 305–125), the other NE–SW (mean strike direction 045–225). A third less pervasive joint set was also mapped. The two sets, which were recognized using both field measurements and lineament mapping are related to regional-scale structures. Joint set J1 is oriented normal to the fold axis of the regional-scale Doldenhorn fold and follows the dominant NW–SE-striking regional structures. Set J2 is orthogonal to set J1, is oriented roughly parallel to the axis of the recumbent fold and parallels the NE–SW-striking normal faults (Kellerhals and Isler 1998).

Deposits

Rock avalanche deposits cover vast parts of the floor of Kandertal (~ 10 km²) in the reach between Kandersteg and Reckenthal (Fig. 4). Based on clear landform contrasts, we subdivide the deposits into three morphological sectors (Fig. 7): (1) the southern proximal sector in the area of the village of Kandersteg and Uf der Höh (local name of the hill formed of landslide debris) in which we also include the Kandersteg basin to the east and the landslide deposits at Schattwald, (2) the middle sector roughly around Blausee and (3) the northern sector, which extends to just north of Reckenthal.

Southern sector

The southern sector is dominated by the main compact body of landslide debris, the 2-km-long, 0.6–0.7-km-wide hill, known as Uf der Höh (Fig. 7). There, the landslide body rises 160 m above the present floodplain of the Kander River (roughly at 1180 m a.s.l.). The core 91/1 log indicates that the landslide debris is in total 200–250 m thick and is underlain by alluvium interbedded with another blocky deposit (Kellerhals and Isler 1998). The contact of the Uf der Höh rock avalanche debris body with the bedrock on the western side of the valley is a 600-m-long, 2–12-m-deep slope-parallel depression, with several parallel ridges. The Uf der Höh landslide debris body has many secondary scarps within it. The most conspicuous is a 500-m-long, N–S-oriented secondary scarp (Fig. 8e). There are also several E–W-directed secondary scarps

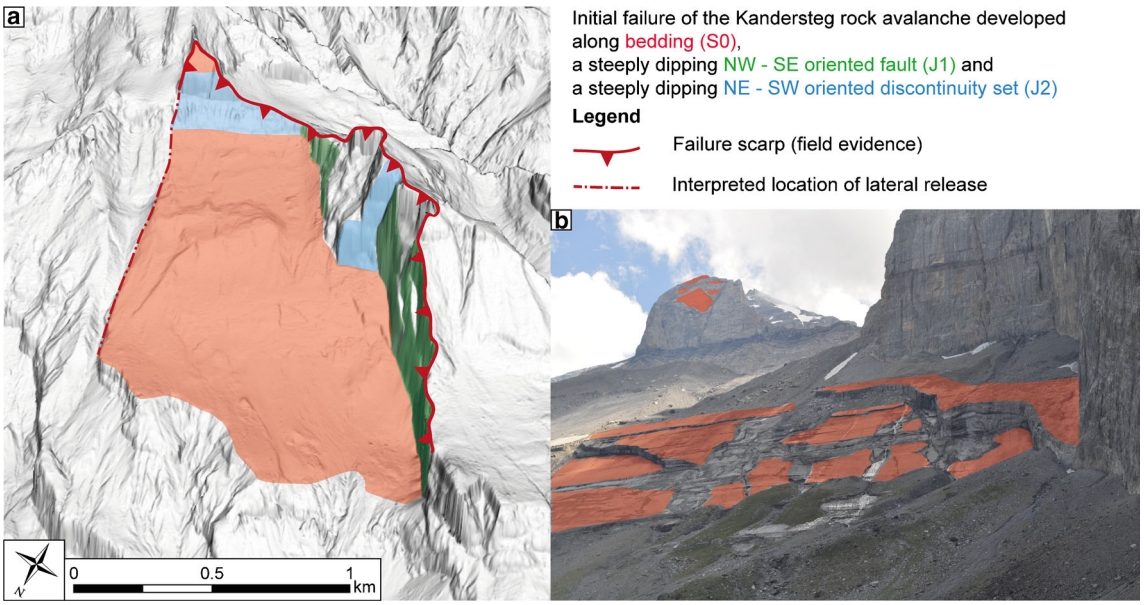

Fig. 6 Structural control of the Fisistock release area. **a** Lateral release was controlled by a steeply dipping fault. Location of back scarp was controlled by both bedding-parallel (S0) and NE–SW-oriented discontinuities (J2). Large parts of the sliding plane follow the orientation of bedding (S0). **b** Basal failure surface is irregular with a stepped geometry, which is in part obscured through erosion and deposition of talus and glacial sediments. Width of basal plane in photo (orange surface) is approximately 250 m. View is to the southeast (photo: C. Singeisen 2016)

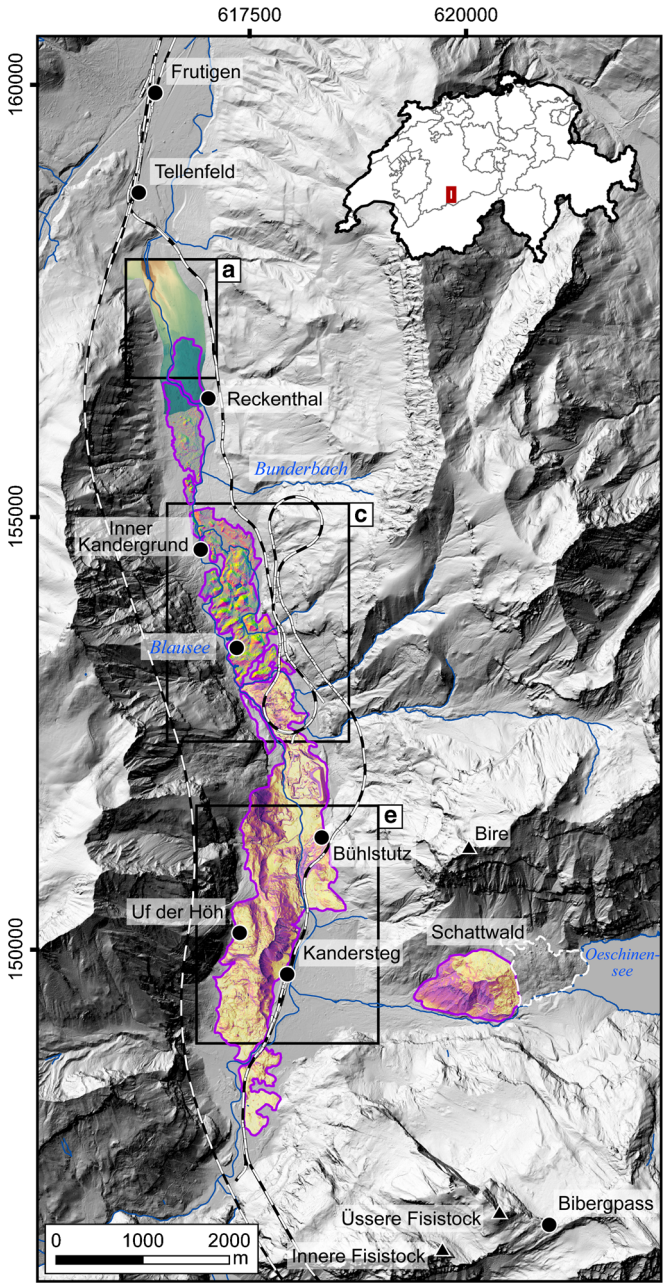

Fig. 7 Overview of Kandersteg region, with locations discussed in text shown. Rectangles indicate areas covered in Fig. 8 a (northern sector), c (middle sector), e (southern sector). Colour coding shown in Fig. 8. Purple line encircles Kandersteg rock avalanche deposits, including Schattwald; white dashed line shows extent of Oeschinensee rock avalanche deposits (Köpfli et al. 2018)

along the southern part of Uf der Höh. Just west of the village of Kandersteg, a 500-m-long, 100-m-high outcrop provides an excellent view of the internal structure of the landslide deposit (Fig. 8f). Apart from the top 1–2 m of sediment, the outcrop is made up of crushed and pulverized Oehrlikalk limestone. The material is very poorly sorted, with grain sizes ranging from silt to blocks of ~ 1 m in diameter. The sediment is a slightly silty sandy gravel with blocks (USCS classification) with very angular to angular clasts. Blocks are infrequent and appear to be floating in a matrix of shattered rock. This is topped by a block facies comprising hundreds of angular to sub-angular megablocks. Lithologies of the boulders at the surface are Kieselkalk and Bänderkalk, and rarely Oehrlikalk (Fig. 9). Average block diameter is 2–3 m, with many reaching more than 10 m. The boulders are densely spaced making the deposit here open framework, although soil is filling many of the gaps. Exposure ages for five boulders from this area are 2.98 ± 0.19 ka (Kander 5), 3.00 ± 0.28 ka (Kander 4), 3.28 ± 0.19 ka (Kander 2), 3.30 ± 0.21 ka (Kander 1) and 4.33 ± 0.29 ka (Kander 6) (Fig. 4).

Most parts of the town of Kandersteg are built on the flat to gently westward sloping terrain of the 2-km-long Oeschibach debris-flow fan and the alluvium of the Kander River. Based on boreholes 91/1 (Kandersteg) and 91/5 (Oeschinensee) (locations in Fig. 4), landslide material should lie below the alluvium of the Kandersteg basin. However, none of the boreholes here in the Kandersteg basin (all < 30 m depth) reached below the alluvium. Today's topography in the area west of the town of Kandersteg is dominated by the levees and channels of the Oeschibach debris-flow fan, which was built up during Oeschinensee lake outburst floods, as for example happened in 1846 AD (Knapp et al. 2018).

A large body of rock avalanche debris is located in the region called Schattwald (Figs. 4 and 7). Exposures in steep erosional scarps formed due to undercutting by the Oeschibach stream reveal that, similar to Uf der Höh, internally the Schattwald hill is composed of rare blocks of Oehrlikalk in a matrix of comminuted Oehrlikalk (cf. Turnau 1906; Köpfli et al. 2018). Infrequent Kieselkalk boulders dot the surface (Fig. 9). No boulders suitable for exposure dating were found.

Middle sector

We placed the boundary between the southern and middle sectors at Bühlstutz (Figs. 4 and 7), where the elevation of the top of the debris body drops from 1170 to 1040 m a.s.l. Here, there is a change from a compact and thick landslide body to a thinner deposit. Based on the interpretation of seismic data, Kellerhals and Isler (1998) inferred a bedrock high with an elevation of 950–1000 m a.s.l. just south of the narrowing of the valley near Bühlstutz. There are no exposures of bedrock in the 35-m-deep gorge of the Kander River at Bühlstutz (Turnau 1906; Furrer et al. 1993).

The middle sector is dominated by sub-parallel transverse ridges with several hummocks (region of Blausee, Fig. 8c). The transverse ridges are up to 30 m high, 70 m wide and 100–250 m long. They are generally oriented perpendicular to flow direction (striking roughly 50°). Gaps of flat topography 40–50 m in width separate the transverse ridges. Blausee and several other small groundwater-fed lakes are located in these gaps. The landscape in this sector is covered with huge (5–10 m diameter) Bänderkalk and Kieselkalk boulders (Fig. 9). A few sandstone boulders, which likely stem from the Tertiary sandstone found at the top of the exposed lateral scarp in the source area, are also present. Exposure ages from boulders in the Blausee region are 3.55 ± 0.55 (Kander 7) and 3.13 ± 0.21 ka (Kander 8).

Northern sector

The transition from the middle to the northern sector occurs in the region of Inner Kandergrund (Fig. 4). The northern sector is dominated by smoothly undulating terrain with

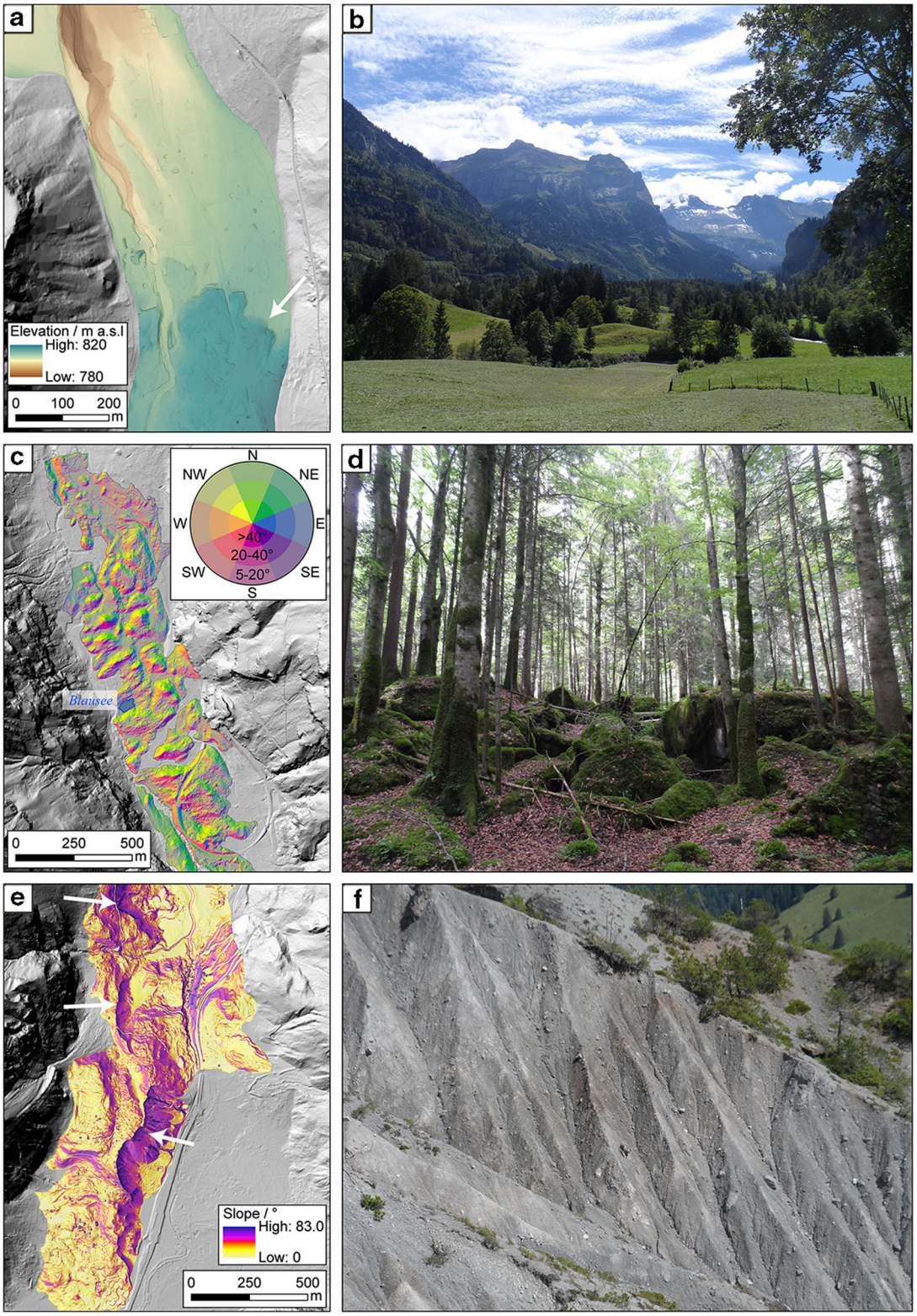

Fig. 8 Details of landforms and deposits of Kandersteg rock avalanche deposits, arranged from north to south (locations shown in Fig. 7). **a** Northern sector, view of distal end of deposits that likely moved in a more fluidized manner than the main part of the landslide to the south. Abrupt toe of the Kandersteg deposit is well visible (arrow). Note active channel of Kander and paleochannels to the east. **b** Photo of hummocky topography in the transitional area between the pull-apart ridge zone (around Blausee, middle sector) and the northern fluidized zone (northern sector). Fisistock and rock avalanche source area visible in background. **c** Slope-aspect map of the middle sector of the deposits highlighting numerous sub-parallel, pull-apart ridges oriented perpendicular to flow direction, especially around Blausee. **d** Photo of the bouldery landscape in the region of Blausee. **e** Slope map of the southern sector, Uf der Höh region. Prominent secondary scarps in the deposits are indicated with arrows. Steep scarp on east side of Uf der Höh (location of outcrop shown in photo f) indicated by lower arrow. **f** Photo of shattered, brecciated sediment exposed at Uf der Höh outcrop (lower arrow in **e**)

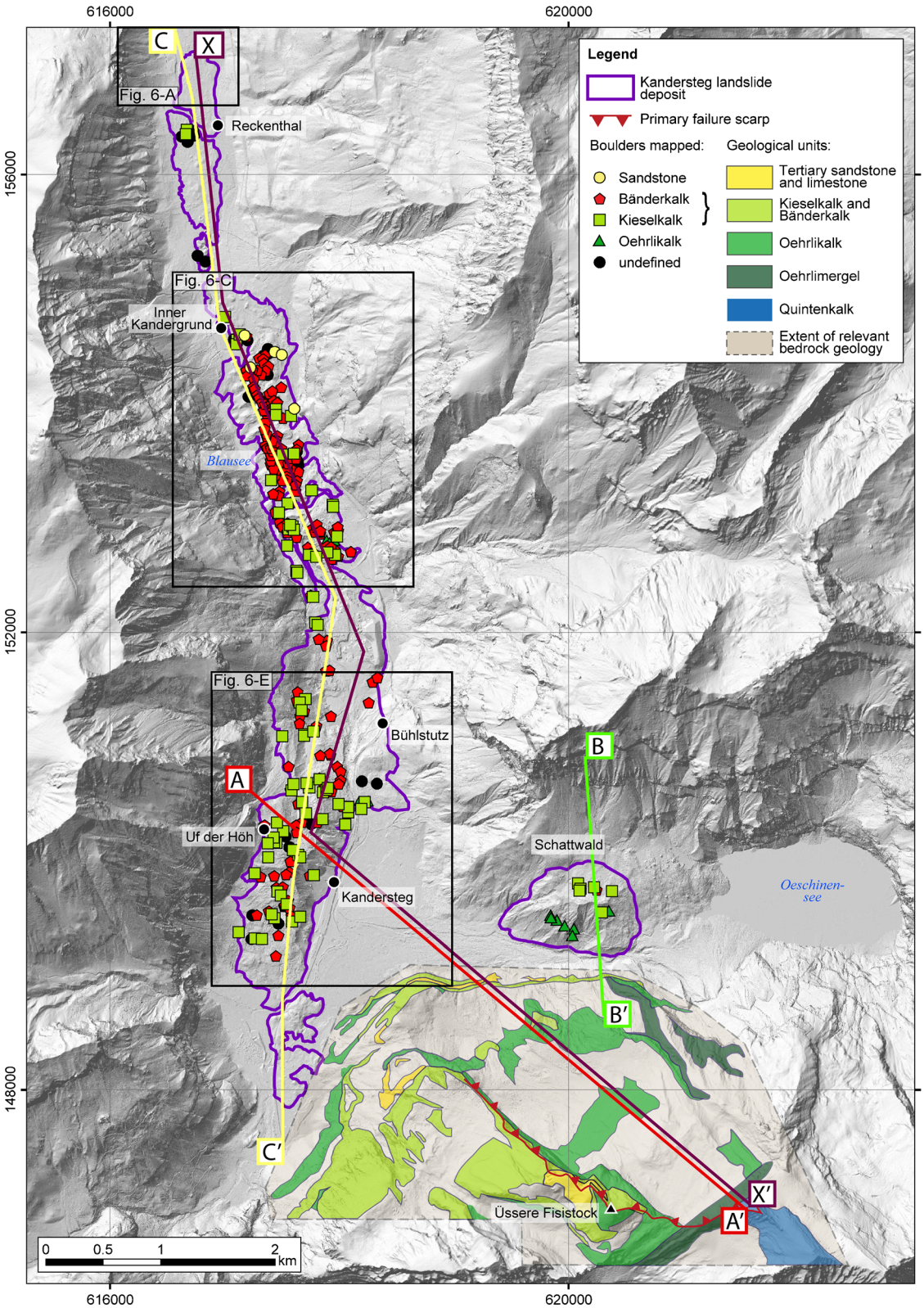

Fig. 9 Lithology of boulders in Kandersteg rock avalanche deposits determined on hand samples and thin sections. Not all boulders could be definitively assigned to a lithology (undefined lithology on map). Also shown are primary failure scarp and bedrock lithologies in the rock avalanche release area (Furrer et al. 1993). Traces of profiles in Figs. 11 and 12 shown

numerous up to 10-m-high hummocks (Fig. 8b). Very few boulders are found in this area. Those that are present are mostly Kieselkalk (diameters < 5 m) (Fig. 9). Here the thickness of the deposit has been estimated to be no more than 20 m (Kellerhals and Isler 1998). The transition from the middle to northern sector is smooth and transitional. The Kandersteg rock avalanche deposits end just north of Reckenthal as marked by the abrupt 5–10-m topographic step of the tongue-shaped toe (Fig. 8a).

Volume estimation and runout modelling

Estimation of the Kandersteg rock avalanche volume

We estimated the volume of the rock avalanche in the source region by reconstructing the missing block on the NW face of Fisistock. The head scarp was interpreted to follow the lithological contact between the Oehrlimergel and Oehrlikalk limestone. The southwestern lateral scarp of the release area is well-defined by a high, steep rock wall. The northeastern lateral edge of the release area is assumed to have been formed by a steep rock wall similar to today's southwestern lateral scarp of the release area. Using these boundaries, the source volume was estimated to be about 750 Mm^3. This number should be regarded as a lower estimate of the failed rock volume. A possible continuation of the pre-failure Fisistock ridge towards the northeast was not taken into account and the actual topography of the failed block cannot be known. Nevertheless, we have taken a parsimonious approach, using the simplest form of the failed block that is in accordance with the present topography and field observations.

Estimation of the volume of the deposit requires knowledge of its thickness. One of the cores taken for the recently constructed Lötschberg base tunnel, 91/1 (location Fig. 4), penetrated below the rock avalanche deposits (Kellerhals and Isler 1998; Ziegler and Isler 2013). The base of landslide debris in borehole 91/1 (surface core elevation 1177 m a.s.l.) occurs at 1066 m a.s.l. Core logs indicate that beneath the landslide deposit, the valley is filled with fluvial, glaciofluvial and glacial sediments, as well as blocky deposits interpreted as an older landslide. We assumed steep valley sides typical of a glacially sculpted U-shaped valley, also in accordance with the bedrock top surface reconstructed by Kellerhals and Isler (1998). The top of the bedrock is at 823.4 m a.s.l. in core 91/1.

For our volume estimation, we include the Schattwald deposits in the Kandersteg event. In core 91/5 (surface elevation 1294.9 m a.s.l., location shown in Fig. 4), Kellerhals and Isler (1998) logged 90 m of landslide deposits underlain by talus and debris-flow sediments. The base of this landslide deposit is at 1203.9 m a.s.l. in core 91/5. Accordingly, we infer a gradually sloping paleolandscape surface from Oeschinental to Kandertal, as defined by the base of the landslide deposits in the two cores (1066 m a.s.l. in 91/1 and 1203.9 m a.s.l. in 91/5). We also assumed a gradually sloping pre-slide valley floor northwards from Kandersteg to the toe of the deposits north of Reckenthal. The resulting volume of the deposit is 1100 Mm^3. If neither the Schattwald deposits nor the postulated landslide deposits beneath the Oeschibach fan and Kandersteg basin (Figs. 4 and 7) are included, an approximate volume of 350 Mm^3 is obtained. This is much less than the estimated source area volume (750 Mm^3).

DAN3D runout modelling

We found that the Kandersteg rock avalanche could best be modelled using a Voellmy basal rheology. The best estimate of runout was achieved with the following input parameters: $\mu = 0.4$, $\xi = 400$ m/s² for surrounding bedrock, $\mu = 0.13$, $\xi = 500$ m/s² for the sliding plane itself and $\mu = 0.04$, $\xi = 800$ m/s² for the valley fill, with bulking and entrainment. For comparison, Hungr and Evans (1996) and Hungr and Hungr and McDougall (2006) recommend values of $\mu = 0.1$ and $\xi = 500$ m/s² for rock avalanche propagation on a valley floor without a glacier present. Our back-analysed parameters fit within the range of accepted values (Hungr and Evans 1996; Sosio et al. 2008; Schleier et al. 2017; Spreafico et al. 2018). A relatively high friction coefficient was used for the underlying bedrock in the Kandersteg simulations to reduce velocities in the extremely steep terrain. Sensitivity analysis has shown that the friction coefficient has a stronger control on runout distance and was hence mainly used to calibrate the back-analysis of the runout, whereas the turbulence coefficient is strongly correlated with velocity distribution (see also Supplemental Material).

The low friction coefficient (and related low shear strength) of the basal sliding surface likely reflects the presence of a marl layer (Oehrlimergel), which is interbedded with the massive limestone of the Oehrlikalk formation in the Doldenhorn nappe (Kellerhals and Isler 1998). In order to simulate the long runout observed in the field, a relatively low friction coefficient was also required for the valley infill. Although the input value falls within the range of values commonly used to model rock and ice-rock avalanches, the material must have been relatively fluid and must have had a low viscosity.

Figure 10a shows the evolution of the simulated velocity of the rock avalanche with time during the emplacement process in the best of the 80 model runs (see Supplemental Material). It must be noted that the discussed velocities are a model output and may not represent the actual velocities. After initial detachment, the rock mass impacts the valley floor in Oeschinental at 20–30 s. Most of the material that was released until this point is located in the narrow Oeschinental, where the Schattwald deposit is. Material continues to be released between $t = 50$ s and $t = 100$ s. The highest velocities, up to 62 m/s, occur on the sliding plane and directly below it in the area of Kandersteg. At time $t = 100$ s, the landslide starts spreading northwards. The rock avalanche moves downvalley with simulated speeds of up to 32 m/s at the toe. As the landslide moves northwards, the thickness of the deposit decreases (Fig. 10b). The runout of the rock avalanche almost reaches its final position after 400 s, and simulated velocities drop to a maximum of 6.6 m/s at the toe of the landslide. After 600 s, the front of the landslide has come to rest but internal deformation of the mass continues until the end of the model run (2000 s). It is also apparent in the graphs that some landslide material remains close to the steep rock walls in the release area as well as near Oeschinensee.

In Fig. 11, today's topography (blue line) is compared with model results with (i) no entrainment (red line), (ii) with 25% bulking (orange dash–dot line) and (iii) with bulking and substrate entrainment (green dotted line). The most notable difference between all model results and the present topography is that the thick deposits at Uf der Höh do not appear in any of the model outputs. The distribution of the landslide deposits is flat, covering the valley floor with a relatively thin layer of landslide material.

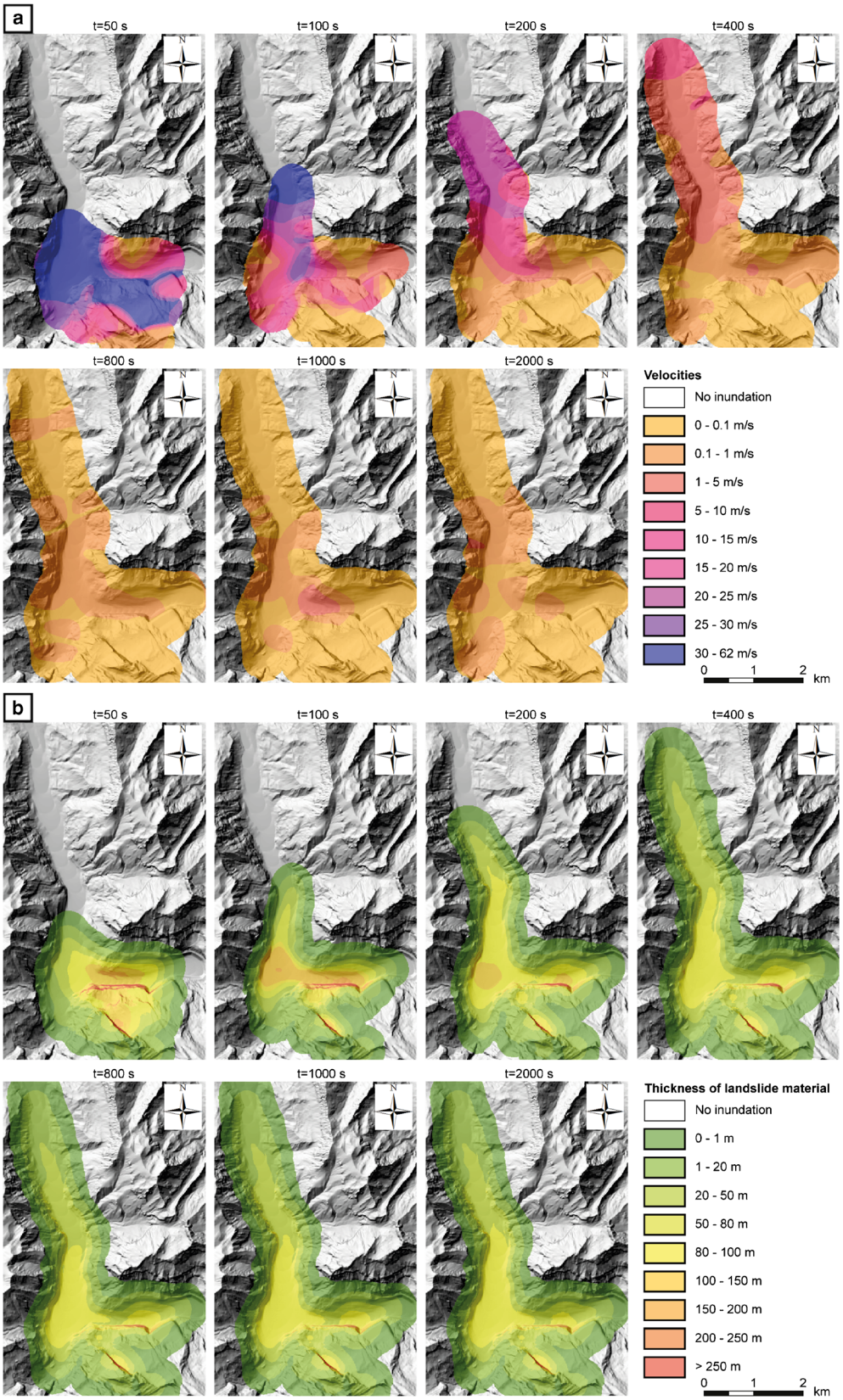

Fig. 10 Results of DAN3D runout modelling for Kandersteg rock avalanche. **a** Modelled peak velocities for specified time step. **b** Modelled thicknesses of the landslide material for specified time step. Results were obtained when modelling the runout of the rock avalanche using the best-fit input parameters determined by back-analysing the length of the runout in the valley

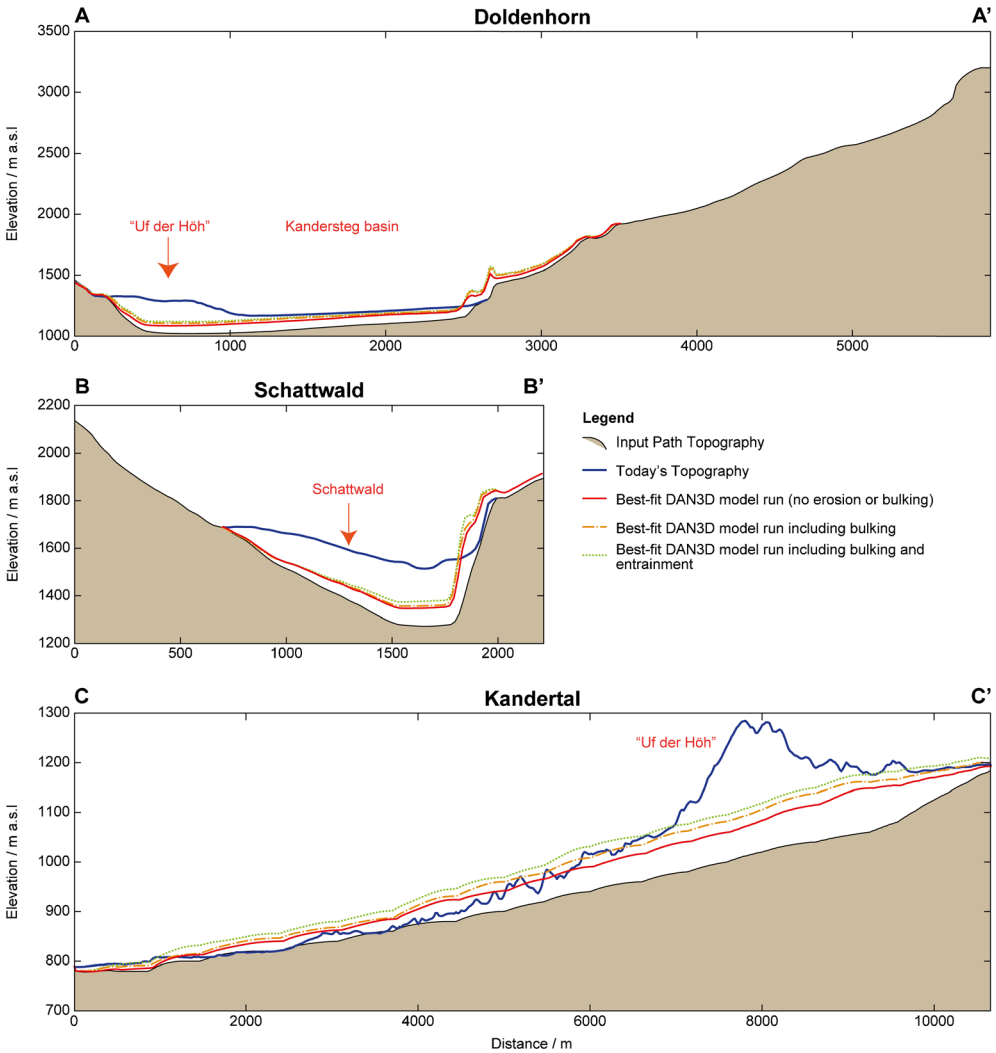

Fig. 11 Comparison of today's topography (blue line) with DAN3D model outputs along three cross-sections A–A′ Doldenhorn, B–B′ Schattwald and C–C′ valley (profile traces shown in Fig. 9). Shaded area indicates the input path topography used for modelling. Note that the thick deposits at Uf der Höh and Schattwald could not be reproduced in the modelling

Similarly, although model results indicate movement northwards (Fig. 10), the model runs do not simulate the thick deposit found at Schattwald. Finally, the DAN3D model results show accumulation of landslide deposits along the foot of the steep rock cliffs below the release area; such deposits are not seen in today's landscape.

Discussion

Sequence of events in Kandertal

The boulder ^{36}Cl exposure ages (Table 1, Fig. 4) vary between 2.98 ± 0.19 ka (Kander 5) and 4.33 ± 0.29 ka (Kander 6), and show no spatial pattern across the deposits. The age of Kander 6 (4.33 ± 0.29 ka) just barely overlaps within the uncertainties with the other ages. We consider this slightly older age to reflect inherited ^{36}Cl, which has been reported from other exposure dated landslide sites (Ivy-Ochs et al. 2009; Martin et al. 2014; Hilger et al. 2019). The mean of the remaining six boulder dates is 3.21 ± 0.22 ka. We found no field evidence in the deposit, such as the presence of a buried soil, which would suggest more than one landslide (cf. Schleier et al. 2017). We concur with Turnau (1906), Nussbaum (1934), Heim (1932) and Abele (1974) that the Kandersteg landslide deposit is the result of a single large catastrophic rock slope failure from the obvious niche at Fisistock. The dates obtained from the bedrock surfaces, 1.71 ± 0.10 and 1.94 ± 0.12 ka, are notably younger than the dates from boulders in the deposit. We consider the bedrock dates to reflect break off of centimetre-thick slabs from the bedding planes after the main catastrophic event, as similarly interpreted at Lavini di Marco by Martin et al. (2014). We note that the basal plane is stepped and that the Oehrlimergel is interbedded with the Oehrlikalk at its base, enhancing probability of later detachment of thin plates. It is also difficult to rule out that the sampled bedrock surfaces may have been intermittently covered by scree, which is abundant on the slope, or snow, both of which would lower the age. Too young ages, attributed to shielding by soil and periodically snow, are reported from bedrock surfaces in the release area at the Flims landslide (Ivy-Ochs et al. 2009). We do

not consider it likely that the Schattwald deposits are related to the dates from the bedrock surfaces as the former underlie the Oeschinensee rock avalanche deposits which have been dated to 2.3 ka (Köpfli et al. 2018).

Crucial clues about failure and emplacement mechanisms of the Kandersteg rock avalanche are revealed by the geomorphological and structural data obtained in our study. Failure along the NW-facing slope at Fisistock was strongly controlled by the mapped joint sets and the dip slope of the massive limestone. The block that failed detached from the upper recumbent fold limb of the Doldenhorn nappe (Fig. 13). The upper part of the head scarp detachment was along bedding planes in the Oehrlikalk limestone (So) and the steeply NW dipping discontinuity set (J_2). Lateral detachment to the southwest was along the fault we mapped as part of the J_1 discontinuity set (Fig. 6).

Our DAN3D modelling results can be used to understand the changes in dynamic behaviour during the event. The event occurred in several phases: release, sliding, propagation across the Kandersteg basin, impact against the west wall of Kandertal, northward (and southward) spreading and finally fluidization of the frontal sector of the moving mass. This sequence is shown schematically in Fig. 12. The DAN3D model results, as portrayed by the thickness distribution figure (Fig. 10b) show that initially movement was to the north towards Schattwald. However, as the most voluminous deposit is actually found at Uf der Höh, the main direction of propagation was predominantly to the northwest towards Kandersteg. The difference in the simulated and actual main direction of landslide movement might be explained by the fact that the sliding surface is well constrained through topography in the southwest but unconstrained on the northeast side (Fig. 4). This highlights the importance of lateral confinement during initiation. In addition, the DAN3D model assumes a fragmented rock mass from the beginning, thus in the model the mass had already started to spread to the north and northeast at the moment of failure. Movement of the sliding body as a semi-coherent block at initial release is more realistic. Accordingly, in the initial stages the block would have slid in a northwesterly direction following the dip direction of the bedding planes (So), rather than towards the north as seen in our DAN3D results. As it moved down the sliding plane, the mass began to break up and fragments shot over the 600-m-high steep rock walls (Fig. 12b). Part of the landslide moved to the north and hit the opposite valley wall in Oeschinental to form the Schattwald landslide deposit (Fig. 10). Reflecting the immense energy of the collapse, the mass moved rapidly across the Kandersteg plain and impacted the western wall of Kandertal forming the hill Uf der Höh and several compressional ridges. Compressional ridges have been described at the Frank (Brideau et al. 2011) and Madison Canyon slides (Wolter et al. 2016), among others (Shea and de Vries 2008; Shugar and Clague 2011; Guthrie et al. 2012). The DAN3D simulations did not show such a thick accumulation as seen at Uf der Höh, as the parameters we used were more fluid-like to simulate the distal runout.

After impacting the western slope of Kandertal, the mass was then deflected and started spreading both northwards and southwards. This is well represented in the runout model velocity results (Fig. 10a). Numerous secondary scarps in the Uf der Höh area in the southern sector (Fig. 8c) suggest continued instability and readjustment of the debris mass during the late phases of the event. This includes the E–W-oriented (transverse to direction of movement) secondary scarps and related ridges in the southern part of Uf der Höh and the more than 40-m-high secondary scarp to the north (indicated by arrow in Fig. 8e). The latter scarp is oriented N–S, which is parallel to the above described compressional ridge direction suggesting a relaxation response after the initial impact of the debris mass with the western Kandertal valley wall. Timings of continued internal movements obtained from DAN3D simulations appear to agree broadly with the locations of major secondary scarps in the deposit, especially at Uf der Höh. Secondary scarps, such as those observed here at Kandersteg, refer

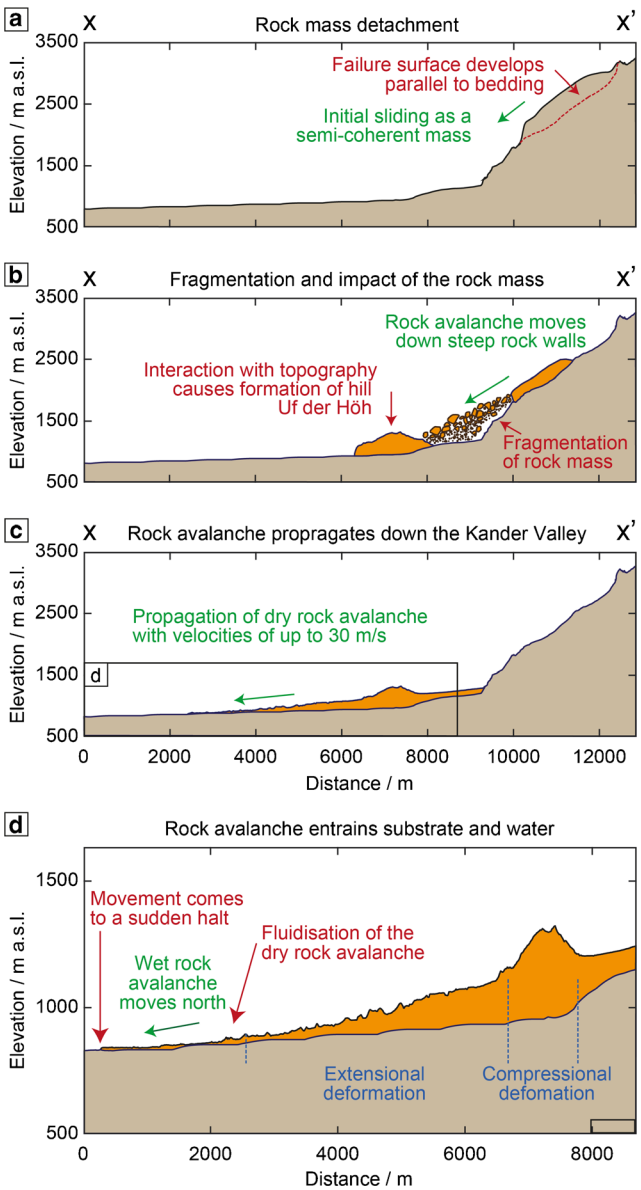

Fig. 12 Longitudinal profile of Kandertal showing the four phases of the Kandersteg rock avalanche emplacement process as interpreted from field observations and runout modelling (profile traces shown in Fig. 9). **a** Failure and initial movement as a semi-coherent block. **b** Disintegration of the rock mass as it shoots over the 600-m-high cliff, followed by build-up of the Uf der Höh deposit near the town of Kandersteg. **c** Propagation to the north. **d** Fluidisation of the toe due to entrainment of wet alluvial sediments. Note change in scale of **d**, close-up of the downstream part of X–X′ shown in black square in profile **c**

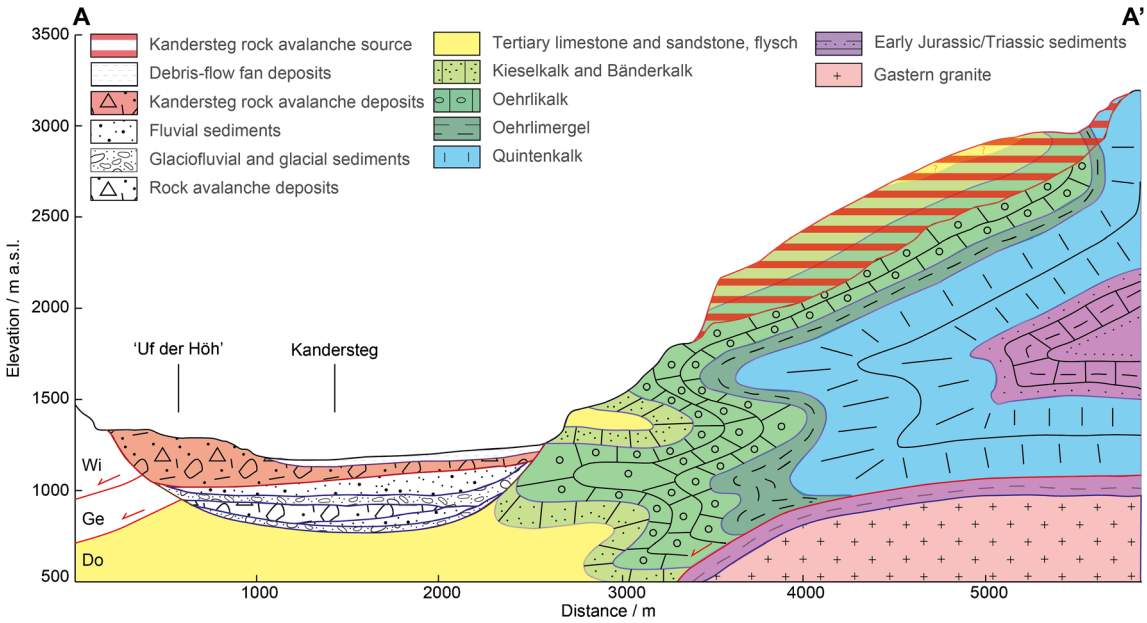

Fig. 13 Schematic geologic cross-section from Kandersteg rock avalanche source area under Fisistock to the hill Uf der Höh. Bedrock structure in the source area is characterized by large-scale recumbent fold of Doldenhorn nappe (modified from Pfiffner 2010). Valley infill includes a lower landslide deposit overlain by fluvial and glaciofluvial (?) sediments and Kandersteg rock avalanche debris (interpreted from core logs in Kellerhals and Isler 1998)

to scarps within the rock avalanche deposit itself (cf. Strom 2006; Hilger et al. 2018) and have been reported from several sites, for example at the U-turn slide in the Mackenzie Mountains (Eisbacher 1979).

The distal landslide debris shows evidence of extensional deformation. Notable are the hundred-meter-long transverse ridges with flat intervening valleys akin to pull-apart ridges, best expressed in the Blausee region (middle sector) (Fig. 8c). These form as a result of tensile stresses within the rock avalanche body as described by several authors (Strom 2006; Shea and de Vries 2008; Wang et al. 2018). Hummocks in distal regions develop if the frontal part of the rock avalanche emplaces faster than the rest of the landslide body (Dufresne and Davies 2009; Paguican et al. 2014), as for example at the Obernberg rock avalanche (Ostermann et al. 2012). We suggest that the smooth, undulating terrain in the northern sector (Reckenthal) formed as a water-rich mass movement during the Kandersteg event (Fig. 8a). The next phase of the emplacement is, therefore, envisioned as a transition from a dry to a wet rock/debris avalanche, or even debris flow, as the material propagated northwards (Fig. 12c). At the time of the event, the valley floor was likely swampy with a meandering Kander River. Wet sediments incorporated at the base of the moving debris mass enhanced mobility contributing to the excessive runout (Aaron and McDougall 2019). It is therefore proposed that the entrainment of water-rich sediments caused acceleration of the landslide movement, which favoured the development of extensional hummocks, akin to pull-apart ridges, described in the middle sector. Acceleration of the toe is well represented in the modelling as shown in the velocity results (Fig. 10a). Finally, the abrupt 5–10-m-high landscape step in the terminus of the deposit (Fig. 8a) suggests that movement came to a sudden halt (Dufresne and Davies 2009). Transition from dry grain flow to wet rock/debris avalanche as reflected in surface morphology has been described at the Cheam rock avalanche (Orwin et al. 2004), at the 1965 Hope Slide (Mathews and McTaggart 1969) and at the 2010 Mount Meager failure that transitioned into a debris flow (Guthrie et al. 2012).

Additional insight into emplacement and propagation processes is gained from sedimentological evidence (Dunning et al. 2005; McSaveney and Davies 2006; Dunning and Armitage 2011; Weidinger et al. 2014; Dufresne et al. 2016; Schleier et al. 2017). The comminuted sediment in the main body of the Kandersteg rock avalanche deposit at Uf der Höh (Fig. 8f), which we recognize as the 'body facies' (sensu Dunning et al. 2005; Weidinger et al. 2014; Dufresne et al. 2016), supports our interpretation of emplacement as a dry rock avalanche in the southern sector. The extreme degree of fragmentation (predominance of silt and sand-sized fragments over the rare 1–2-m clasts, Fig. 8f) is in line with high energy during movement, which is also reflected in the high velocities obtained in the modelling (Fig. 10a). Similar interpretations have been made from sedimentological studies at other Alpine rock avalanches, for example at Flims and Tschirgant (Dunning and Armitage 2011; Dufresne et al. 2016). The overlying megablock part of the deposit, the 'carapace' or hard shell (Dunning et al. 2005; Weidinger et al. 2014; Dufresne et al. 2016), which is observed in both the southern and middle sectors but not in the northern, indicates passive transport of the huge blocks on top of the fragmenting moving mass. The sequence, crushed sediment derived from Oehrlikalk of the body facies underlying Kieselkalk blocks of the carapace, mimics the stratigraphic order in the bedrock of the release area (Fig. 2). In addition, it seems that the Oehrlikalk behaved in a more brittle manner than the Kieselkalk rock fragments. The former underwent extensive pulverization during emplacement, while the latter remained as several meter-diameter blocks in the carapace.

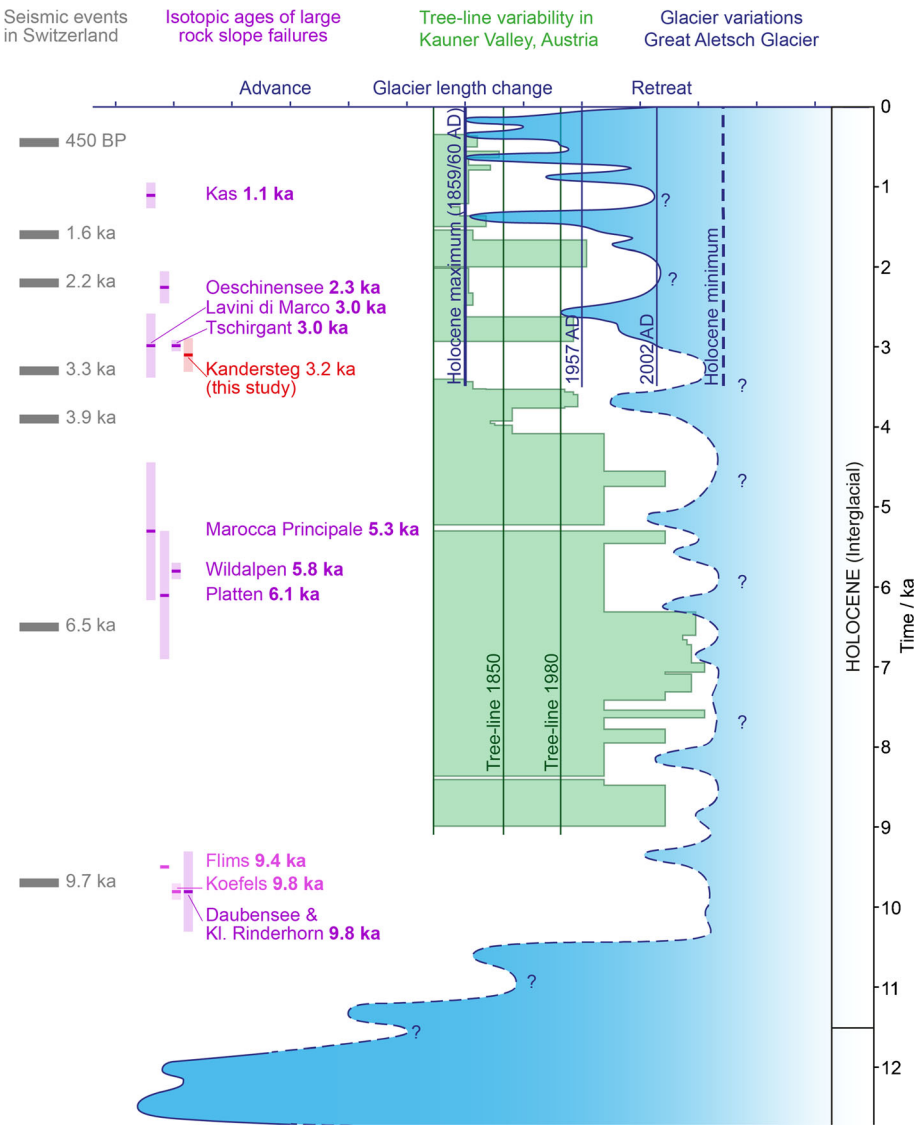

Fig. 14 Timing of the Kandersteg rock avalanche in relation to the glacier variations (modified from Ivy-Ochs et al. 2009, Grämiger et al. 2017 and references therein) and lake record-derived seismic events in Switzerland (Kremer et al. 2017). For comparison, isotopic dates for other large mass movements in the Alps are shown (site locations in Ivy-Ochs et al. 2017). Glacier variations time-distance diagram on relative distance scale. Great Aletsch Glacier data from Holzhauser (1995); treeline data from Nicolussi et al. (2005)

In the Fisistock release area Oehrlikalk, Kieselkalk, Bänderkalk and Tertiary sandstone are exposed from bottom to top (Fig. 2). The boulder lithology distribution in the deposits generally reflects this order from proximal to distal (Fig. 9). Thus, the stratigraphic sequence was preserved with the top lithologies travelling farthest. Strom (2006) discusses development of stratified bodies with preservation of source stratigraphy from proximal to distal in the Kokomeren, Inylchek and Blackhawk landslides. The preserved bedrock stratigraphy in the spatial distribution of boulder lithologies also supports the hypothesis of a single landslide event (cf. Charrière et al. 2016).

It may be that a landslide-dammed lake was created in the Kandersteg basin as a result of the Kandersteg rock avalanche (Turnau 1906; Beck 1929, 1952; Tinner et al. 2005). However, as there is neither morphological nor sedimentological evidence for a long-lasting paleolake in the Kandersteg basin, Turnau (1906) suggested that the lake overtopped and breached the deposit soon after the event, creating today's Kander River gorge (visible SW of Bühlstutz on Fig. 7). In contrast, Beck (1929, 1952) and Tinner et al. (2005) made the interpretation that the northernmost part of the deposit (our northern sector) was formed through catastrophic breaching of a landslide dam and an outburst flood from a lake that existed for several hundred years. We find no morphological evidence for this in the deposits we have studied. Catastrophic breaching of a landslide dam would have resulted in a massive debris flow that would have flowed over the hummocky terrain and left geomorphological evidence of its passing. In reality, the hummocky, unequivocally primary landslide terrain (Fig. 8b), between the proposed location of the landslide dam (i.e. just north of the area Uf der Höh) and the abrupt toe (Fig. 8a, northern

sector), is well preserved and has not been modified by overtopping of a later debris flow. The gradual transition from hummocky to smoothly undulating terrain in the distal region points to a single event.

Cosmogenic surface exposure dating carried out in this study reveals an age of 3.21 ± 0.22 ka for the extensive rock avalanche deposits that cover much of the Kandertal valley floor. This age is notably younger than the previously proposed age of 9.6 ka (Tinner et al. 2005), derived from radiocarbon dating of organic material from sites near Frutigen (Fig. 1). Data from core 91/1 (location shown in Fig. 4) indicate that the Kandersteg rock avalanche deposit is underlain by fluvial sediments which in turn are underlain by another blocky (landslide) deposit (Fig. 13). The latter may correlate to the deposits further downstream studied by Tinner et al. (2005).

Conditioning and triggering

Our data point to a single, roughly 1-km^3 event at 3.21 ± 0.22 ka sourced at Fisistock. Previous work had suggested an age of 9.6 ka (Tinner et al. 2005). This means that the early Holocene 'cluster' of Alpine rock avalanche events in the Alps (Fig. 14) now comprises only Koefels (9.8 ka; Ivy-Ochs et al. 1998; Nicolussi et al. 2015) and Flims (9.4 ka; Deplazes and Anselmetti 2007; Ivy-Ochs et al. 2009). Two smaller landslides at Rinderhorn, located 7 km south of Kandersteg, were dated to 9.6 ka by Grämiger et al. (2016).

Based on the determined exposure ages, the Kandersteg rock avalanche falls into the cluster of mid- to late Holocene landslides in the Alps dated to ca. 5–3 ka (Prager et al. 2008; Martin et al. 2014; Zerathe et al. 2014; Ivy-Ochs et al. 2017 and references therein). Zerathe et al. (2014) suggest that the enhanced frequency in slope activity is related to increasingly wetter conditions after around 4 ka (Fig. 13). Similarly, glaciers in the Alps advanced more frequently beginning at that time, with a 3.6-ka advance dated at several sites (LeRoy et al. 2017; Badino et al. 2018). During these advances, glaciers reached roughly their Little Ice Age extents. As the Doldenhorngletscher just above the Fisistock release area (Fig. 1) was markedly larger during the Little Ice Age (based on historical maps), it may have reached a similar extent 3.6 ka ago and therefore covered the top parts of the Kandersteg source area. Glacial erosion would have weakened the back-scarp area, allowed water infiltration and freezing along fractures and bedding planes and contributed to rock mass destabilization and ultimately to failure (Gruber and Haeberli 2007; Huggel et al. 2010). The upper reaches and the steep north-facing side wall of the release area are presently in the permafrost zone (Boeckli et al. 2012; Kenner 2017). During cold climate pulses of the Little Ice Age, permafrost extended many tens of meters lower in elevation (Lambiel and Reynard 2001). Air temperature fluctuations (1–2 °C) related to late Holocene climate variations and concomitant alternating freezing and thawing of rock permafrost resulted in a decrease of strength along pre-existing discontinuities and rock mass fatigue (Moore et al. 2011; Krautblatter et al. 2013). Finally, the close spacing of joints in the fault zone along the western lateral scarp could have favoured the penetration of water and led to increased weathering of joints and build-up of pore pressure. The presence of karst may have weakened the rock mass further (cf. Pánek et al. 2009), contributed to water infiltration and redistribution and affected pore water pressure changes (Santo et al. 2007; Parise 2008; Yin et al. 2011; Krautblatter et al. 2012). Caves occur in the Fisistock area, as for example the Seehöhle cave within the Oehrlikalk (Wildberger and Preiswerk 1997). Notably, Pesendorfer and Loew (2004) documented an extensive karst system in the rocks of the Doldenhorn nappe during construction of the Lötschberg base tunnel (tunnel trace shown in Fig. 1). All of these factors, many of which still exist today, contributed to destabilization of the slope. Frequent rock fall activity occurs even today along the impressively steep and high lateral release rock wall. At the time of this writing, the Spitze Stei just outside the Kandersteg source area to the northeast is reported to be moving at a rate of several centimetres per day and is being closely monitored (SRF documentary https://www.srf.ch/play/tv/schweiz-aktuell/video/der-spitze-stein-ueber-kandersteg-rutscht-immer-mehr-bergab).

The young age we determined places the Kandersteg rock avalanche in a completely new context with respect to possible preparatory and triggering factors. It is striking that a seismic event with an age of 3.3 ka was identified by Kremer et al. (2017, and references therein) based on the study of sediment cores from lakes Seelisberg, Zurich and Lucerne. The event is thought to have been located in eastern Switzerland. The authors estimated a paleomagnitude of Mw > 5.7. The age of the seismic event is strikingly similar to the age of the Kandersteg rock avalanche. Even if the failure was not triggered by a single (distant) earthquake, seismic activity, which is still high today with several nearby large-magnitude events in the last 100 years (Fäh et al. 2011; Fritsche et al., 2012), could have led to progressive weakening (fatigue) and preconditioning of the rock mass (Gischig et al. 2016; Moore et al. 2012; Wolter et al. 2016). Köpfli et al. (2018) proposed seismic triggering for the 2300-year-old Oeschinensee rock avalanche (deposits shown on Figs. 4 and 7) by the 2.2-ka seismic event recognized in lakes Geneva, Neuchatel, Lucerne and Zurich (Kremer et al. 2017). Knapp et al. (2018) suggested seismic triggering for several rock-slope failures they studied in Oeschinensee sediments in response to earthquakes at 1755, 1855 and 1946 AD in the Rhone Valley region (Fäh et al. 2011; Fritsche et al. 2012). Hence, although it is difficult to identify the actual trigger for the Kandersteg event, a combination of unfavourable structural setting of the slope, glacially undercut dip slope situation, glacial erosion of the head scarp, frequent temperature variations in the existing permafrost and seismic fatigue likely led to destabilization and failure of the rock mass below the Fisistock.

Conclusions

We have used an integrated approach combining field and remote mapping, dynamic runout modelling and cosmogenic ^{36}Cl exposure dating to decipher the detachment mechanisms, emplacement processes and timing of the Kandersteg rock avalanche. Cosmogenic ^{36}Cl exposure dating indicates that within the dating uncertainties there was one catastrophic event. In concurrence, no field evidence for more than one event was found in the Kandersteg deposits. Our determined ^{36}Cl exposure age of 3.21 ± 0.22 ka from boulders all across the deposit supports the premise of a single colossal event. The Kandersteg event is significantly younger than the previously accepted age of 9.6 ka (Tinner et al. 2005).

Based on field and remote mapping, the rock avalanche (source volume 750–900 Mm^3, deposit volume 1100 Mm^3) failed along dip slope bedding planes (S0) and two discontinuity sets (J1, J2) on the

upper limb of a recumbent fold. Weak marl layers interbedded with massive limestone beds likely formed the basal sliding surface zones. Glacial erosion along the back wall, permafrost degradation, karst and seismic fatigue are other preconditioning factors. The trigger remains unknown but could have been a Mw > 5.7 earthquake that occurred 3.3 ka.

Through dynamic modelling, it was possible to clarify the complex emplacement processes of the event. Model deposit distribution, material properties (low viscosity) and emplacement times and velocities suggest a single, catastrophic event lasting a few minutes, beginning as a translational, semi-coherent rockslide that transitioned into a dry fragmenting rock avalanche, and finally evolved into a highly mobile debris flow-like failure distally due to incorporation of saturated alluvial sediments at the base. This hypothesis is supported by (i) thick landslide deposits at Uf der Höh (southern sector) that likely formed upon impact with the opposite valley slope, (ii) pull apart–like ridges in the hummocky terrain in the Blausee–Kandergrund area (middle sector) and (iii) smoothly undulating terrain with few boulders between Kandergrund and Reckenthal (northern sector) that suggests fluidization.

We present new insights that considerably enhance our understanding of one of the largest rock slope failures in the Alps. Structural analysis and field observations combined with previous studies reveal that large rock slope failures are common in the Kandersteg area. The rare but hazardous occurrence of large rock slope failures should be given special attention with regard to hazard and risk analysis at Kandersteg.

Acknowledgements

We thank S. Wohlwend for help with thin section analysis and J. Aaron, J. Moore and A. Pfiffner for insightful discussions. We appreciate the numerous suggestions of three anonymous reviewers and handling editor M.A. Brideau. The Amt für Geoinformation of the Kanton of Bern kindly provided the 0.5-m LiDAR DEM. All members of the AMS group at the Laboratory for Ion Beam Physics ETH are appreciated for their dedication and support.

Funding information

C. Singeisen's fieldwork was funded by the Swiss Quaternary Society.

References

Aaron J, Hungr O (2016) Dynamic analysis of an extraordinarily mobile rock avalanche in the Northwest Territories, Canada. Can Geotech J 53:899–908. https://doi.org/10.1139/cgj-2015-0371

Aaron J, McDougall S (2019) Rock avalanche mobility: the role of path material. Eng Geol 257:105126. https://doi.org/10.1016/j.enggeo.2019.05.003

Aaron J, McDougall S, Nolde N (2019) Two methodologies to calibrate landslide runout models. Landslides 16:1–14. https://doi.org/10.1007/s10346-018-1116-8

Abele G (1974) Bergstürze in den Alpen: ihre Verbreitung, Morphologie und Folgeerscheinungen. Wissenschaftliche Alpenvereinshefte 25:1–230

Adrian H (1915) Geologische Untersuchungen der beiden Seiten des Kandertales. Eclogae Geol Helv 13:238–351

Agliardi F, Crosta GB, Zanchi A (2001) Structural constraints on deep-seated slope deformation kinematics. Eng Geol 59(1–2):83–102. https://doi.org/10.1016/S0013-7952(00)00066-1

Alfimov V, Ivy-Ochs S (2009) How well do we understand production of ^{36}Cl in limestone and dolomite? Quat Geochronol 4:462–474. https://doi.org/10.1016/j.quageo.2009.08.005

Bachmann I (1870) Die Kander im Berner Oberland: ein ehemaliges Gletscher- und Flussgebiet; Beitrag zur Kenntnis der schweizerischen Quartärbildungen in gemeinfasslicher Darstellung. Dalp, Bern

Badino F, Ravazzi C, Vallè F et al (2018) 8800 years of high-altitude vegetation and climate history at the Rutor Glacier forefield, Italian Alps. Evidence of middle Holocene timberline rise and glacier contraction. Quat Sci Rev 185:41–68. https://doi.org/10.1016/j.quascirev.2018.01.022

Beck P (1929) Vorläufige Mitteilung über die Bergstürze und den Murgang im Kandertal (Berner Oberland). Eclogae Geol Helv 22:155–159

Beck P (1952) Neue Erkenntnisse über die Bergstürze im Kandertal. Eclogae Geol Helv 45:277–280

Bini A, Buoncristiani J, Couterrand S et al (2009) Die Schweiz während des letzteiszeitlichen Maximums (LGM), karte 1:500 000. Bundesamt für Landestopografie swisstopo, Wabern

Boeckli L, Brenning A, Gruber S, Noetzli J (2012) A statistical approach to modelling permafrost distribution in the European Alps or similar mountain ranges. Cryosphere 6:125–140. https://doi.org/10.5194/tc-6-125-2012

Brideau MA, Yan M, Stead D (2009) The role of tectonic damage and brittle rock fracture in the development of large rock slope failures. Geomorphology 103:30–49. https://doi.org/10.1016/j.geomorph.2008.04.010

Brideau MA, Pedrazzini A, Stead D, Froese C, Jaboyedoff M, van Zeyl D (2011) Three-dimensional slope stability analysis of South Peak, Crowsnest Pass, Alberta, Canada. Landslides 8:139–158. https://doi.org/10.1007/s10346-010-0242-8

Brückner E (1897) Die feste Erdrinde und ihre Formen: Ein Abriss der allgemeinen Geologie und der Morphologie der Erdoberfläche. Tempsky, Prag

Charrière M, Humair F, Froese C, Jaboyedoff M, Pedrazzini A, Longchamp C (2016) From the source area to the deposit: collapse, fragmentation, and propagation of the Frank Slide. Geol Soc Am Bull 128:332–351. https://doi.org/10.1130/B31243.1

Clague JJ, Stead D (2012) Landslides: types, mechanisms and modeling. Cambridge University Press, Cambridge

Crosta GB, Frattini P, Fusi N (2007) Fragmentation in the Val Pola rock avalanche, Italian Alps. J Geophys Res Earth Surf 112:1–23. https://doi.org/10.1029/2005JF000455

Deplazes G, Anselmetti FS (2007) Auf den Spuren des Flimser Bergsturzes im Lag la Cauma und Lag Grond. Geosci Actuel Sci Nat 3:46–50

Dufresne A, Davies TRH (2009) Longitudinal ridges in mass movement deposits. Geomorphology 105:171–181. https://doi.org/10.1016/j.geomorph.2008.09.009

Dufresne A, Prager C, Bösmeier A (2016) Insights into rock avalanche emplacement processes from detailed morpho-lithological studies of the Tschirgant deposit (Tyrol, Austria). Earth Surf Process Landf 41:587–602. https://doi.org/10.1002/esp.3847

Dunning SA, Armitage PJ (2011) The grain-size distribution of rock-avalanche deposits: implications for natural dam stability. In: Evans SG et al (eds) Natural and artificial rockslide dams. Springer, Berlin, Heidelberg, pp 479–498

Dunning SA, Petley DN, Rosser NJ, Strom AL (2005) The morphology and sedimentology of valley confined rock-avalanche deposits and their effect on potential dam hazard. In: Hungr O et al (eds) Landslide risk management. CRC press, Boca Raton, pp 691–701

Eisbacher GH (1979) Cliff collapse and rock avalanches (Sturzstroms). Can Geotech J 16:309–334

Eisbacher GH, Clague JJ (1984) Destructive mass movements in high mountains: hazard and management. Geol Surv Can:84–16

Evans SG, Mugnozza GS, Strom AL, Hermanns RL, Ischuk A, Vinnichenko S (eds) (2006) Landslides from massive rock slope failure. Springer, Dordrecht

Fäh D, Giardini D, Kästli P et al (2011) ECOS-09 Earthquake Catalogue of Switzerland Release 2011 Report and Database. Public catalogue, 17.4.2011. Swiss Seismological Service ETH, Zurich

Fellenberg E, Kissling E, Schardt H (1901) Lötschberg- und Wildstrubeltunnel: Geologische Expertise. Mitt Naturforsch Ges Bern:11–131

Fisher R (1953) Dispersion on a sphere. Proc R Soc Lond A 217(1130):295–305

Fort M, Cossart E, Deline P et al (2009) Geomorphic impacts of large and rapid mass movements: a review. Groupe Franç Géomorphol 15:47–64

Fritsche S, Fäh D, Schwarz-Zanetti G (2012) Historical intensity VIII earthquakes along the Rhone valley (Valais, Switzerland): primary and secondary effects. Swiss J Geosci 105:1–18. https://doi.org/10.1007/s00015-012-0095-3

Furrer H, Huber K, Adrian H et al (1993) Geologischer Atlas der Schweiz, Blatt 87, Adelboden. Bundesamt für Wasser und Geologie BWG, Ittigen

Gerber E, Scheidegger AE (1969) Stress-induced weathering of rock masses. Eclogae Geol Helv 62:401–415. https://doi.org/10.5169/seals-163705

Gischig V, Preisig G, Eberhardt E (2016) Numerical investigation of seismically induced rock mass fatigue as mechanism contributing to the progressive failure of deep-

seated landslides. Rock Mech Rock Eng 49:2457–2478. https://doi.org/10.1007/s00603-015-0821-z
Grämiger LM, Moore JR, Vockenhuber C, Aaron J, Hajdas I, Ivy-Ochs S (2016) Two early Holocene rock avalanches in the Bernese Alps (Rinderhorn, Switzerland). Geomorphology 268:207–221. https://doi.org/10.1016/j.geomorph.2016.06.008
Grämiger LM, Moore JR, Gischig VS, Ivy-Ochs S, Loew S (2017) Beyond debuttressing: mechanics of paraglacial rock slope damage during repeat glacial cycles. J Geophys Res Earth Surf 122:1004–1036. https://doi.org/10.1002/2016JF003967
Gruber S, Haeberli W (2007) Permafrost in steep bedrock slopes and its temperature-related destabilization following climate change. J Geophys Res Earth Surf:112. https://doi.org/10.1029/2006JF000547
Guthrie RH, Friele P, Allstadt K et al (2012) The 6 August 2010 Mount Meager rock slide-debris flow, Coast Mountains, British Columbia: characteristics, dynamics, and implications for hazard and risk assessment. Nat Hazards Earth Syst Sci 12:1277–1294. https://doi.org/10.5194/nhess-12-1277-2012
Heim A (1932) Bergsturz und Menschenleben. Fretz & Wasmuth, Zürich
Hermanns RL, Longva O (2012) Rapid rock-slope failures. In: Clague JJ, Stead D (eds) Landslides: types, mechanisms and modeling. Cambridge University Press, Cambridge, pp 59–70
Hermanns RL, Schleier M, Böhme M, Blikra LH, Gosse JC, Ivy-Ochs S, Hilger P (2017) Rock avalanche activity in W and S Norway peaks after the retreat of the Scandinavian Ice Sheet. In: Mikoš M et al (eds) Advancing culture of living with landslides. Springer, Cham, pp 331–338
Hewitt K, Clague JJ, Orwin JF (2008) Legacies of catastrophic rock slope failures in mountain landscapes. Earth Sci Rev 87:1–38. https://doi.org/10.1016/j.earscirev.2007.10.002
Hilger P, Hermanns RL, Gosse JC, Jacobs B, Etzelmüller B, Krautblatter MJTH (2018) Multiple rock-slope failures from Mannen in Romsdal Valley, western Norway, revealed from Quaternary geological mapping and ^{10}Be exposure dating. Holocene 28:1841–1854. https://doi.org/10.1177/0959683618798165
Hilger P, Gosse JC, Hermanns RL (2019) How significant is inheritance when dating rockslide boulders with terrestrial cosmogenic nuclide dating?—a case study of an historic event. Landslides 16:729–738. https://doi.org/10.1007/s10346-018-01132-0
Holzhauser H (1995) Gletscherschwankungen innerhalb der letzten 3200 Jahre am Beispiel des grossen Aletsch- und des Gornergletschers. Neue Ergebnisse. In: Gletscher im ständigen Wandel. Publikationen der Schweizerischen Akademie der Naturwissenschaften 6:101–123
Huggel C, Salzmann N, Allen S et al (2010) Recent and future warm extreme events and high-mountain slope stability. Phil Trans R Soc Lond A 368(1919):2435–2459. https://doi.org/10.1098/rsta.2010.0078
Hungr O (1995) A model for the runout analysis of rapid flow slides, debris flows, and avalanches. Can Geotech J 32(2):610–623. https://doi.org/10.1139/t95-063
Hungr O, Evans SG (1996) Rock avalanche runout prediction using a dynamic model. In: Senneset K (ed) Proceedings of the 7th International Symposium on Landslides. Balkema, Rotterdam, pp 233–238
Hungr O, Evans SG (2004) Entrainment of debris in rock avalanches: an analysis of a long runout mechanism. Geol Soc Am Bull 116:1240–1252. https://doi.org/10.1130/B25362.1
Hungr O, Mcougall S (2009) Two numerical models for landslide dynamic analysis. Comput Geosci 35(5):978–992. https://doi.org/10.1016/j.cageo.2007.12.003
International Society for Rock Mechanics Commission on Standardisation of Laboratory and Field Tests (ISRM) (1978) Suggested methods for the quantitative description of discontinuities in rock masses. Int J Rock Mech Min Sci Geomech Abstr 15:319–368
Ivy-Ochs S (2015) Glacier variations in the European Alps at the end of the last glaciation. Cuad Investig Geog 41:295–315
Ivy-Ochs S, Heuberger H, Kubik PW, Kerschner H, Bonani G, Frank M, Schlüchter C (1998) The age of the Köfels event-relative, 14C and cosmogenic isotope dating of an early Holocene landslide in the Central Alps (Tyrol, Austria). Z. Gletsch.kd. Glazialgeol 34:57–68
Ivy-Ochs S, Synal HA, Roth C, Schaller M (2004) Initial results from isotope dilution for Cl and ^{36}Cl measurements at the PSI/ETH Zurich AMS facility. Nucl Instrum Meth B 223:623–627. https://doi.org/10.1016/j.nimb.2004.04.115
Ivy-Ochs S, Poschinger A, Synal HA, Maisch M (2009) Surface exposure dating of the Flims landslide, Graubünden, Switzerland. Geomorphology 103:104–112. https://doi.org/10.1016/j.geomorph.2007.10.024
Ivy-Ochs S, Martin S, Campedel P et al (2017) Geomorphology and age of the Marocche di Dro rock avalanches (Trentino, Italy). Quat Sci Rev 169:188–205. https://doi.org/10.1016/j.quascirev.2017.05.014
Jaboyedoff M, Couture R, Locat P (2009) Structural analysis of Turtle Mountain (Alberta) using digital elevation model: toward a progressive failure. Geomorphology 103:5–16. https://doi.org/10.1016/j.geomorph.2008.04.012
Kellerhals P, Isler A (1998) Lötschberg-Basistunnel: Geologische Voruntersuchungen und Prognose. Geologische Berichte Nr. 22, Landeshydrologie und Geologie, Bern
Kenner R (2017) Permafrost and ground ice map of Switzerland [data set]. Zenodo. https://doi.org/10.5281/zenodo.803850
Knapp S, Gilli A, Anselmetti FS, Krautblatter M, Hajdas I (2018) Multistage rock-slope failures revealed in lake sediments in a seismically active Alpine region (Lake Oeschinen, Switzerland). J Geophys Res Earth Surf 123:658–677. https://doi.org/10.1029/2017JF004455
Köpfli P, Grämiger LM, Moore JR, Vockenhuber C, Ivy-Ochs S (2018) The Oeschinensee rock avalanche, Bernese Alps, Switzerland: a co-seismic failure 2300 years ago? Swiss J Geosci 111:205–219. https://doi.org/10.1007/s00015-017-0293-0
Körner H (1976) Reichweite und Geschwindigkeit von Bergsturzen und Fliessschneelawinen. Rock Mech 8:225–256
Korup O, Densmore AL, Schlunegger F (2010) The role of landslides in mountain range evolution. Geomorphology 120(1):77–90. https://doi.org/10.1016/j.geomorph.2009.09.017
Krautblatter M, Huggel C, Deline P, Hasler A (2012) Research perspectives for unstable high-alpine bedrock permafrost: measurement, modelling and process understanding. Permafrost Periglac 23:80–88. https://doi.org/10.1002/ppp.740
Krautblatter M, Funk D, Günzel FK (2013) Why permafrost rocks become unstable: a rock–ice-mechanical model in time and space. Earth Surf Process Landf 38(8):876–887. https://doi.org/10.1002/esp.3374
Krebs J (1925) Stratigraphie der Blüemlisalp-Gruppe: Fisistock-Doldenhorn-Blümlisalp-Gspaltenhorn im Berner Oberland. Stämpfli, Bern
Kremer K, Wirth SB, Reusch A, Fäh D, Bellwald B, Anselmetti FS, Girardclos S, Strasser M (2017) Lake-sediment based paleoseismology: limitations and perspectives from the Swiss Alps. Quat Sci Rev 168:1–18. https://doi.org/10.1016/j.quascirev.2017.04.026
Lambiel C, Reynard E (2001) Regional modelling of present, past and future potential distribution of discontinuous permafrost based on a rock glacier inventory in the Bagnes-Hérémence area (Western Swiss Alps). Nor Geogr Tidsskr 55(4):219–223. https://doi.org/10.1080/00291950152746559
Leith K, Moore JR, Amann F, Loew S (2014) Subglacial extensional fracture development and implications for Alpine valley evolution. J Geophys Res Earth Surf 119(1):62–81. https://doi.org/10.1002/2012JF002691
LeRoy M, Deline P, Carcaillet J, Schimmelpfennig I, Ermini M, ASTER Team (2017) ^{10}Be exposure dating of the timing of Neoglacial glacier advances in the Ecrins-Pelvoux massif, southern French Alps. Quat Sci Rev 178:118–138. https://doi.org/10.1016/j.quascirev.2017.10.010
Marrero SM, Phillips FM, Caffee MW, Gosse JC (2016) CRONUS-Earth cosmogenic ^{36}Cl calibration. Quat Geochronol 31:199–219. https://doi.org/10.1016/j.quageo.2015.10.002
Martin S, Campedel P, Ivy-Ochs S et al (2014) Lavini di Marco (Trentino, Italy): ^{36}Cl exposure dating of a polyphase rock avalanche. Quat Geochronol 19:106–116. https://doi.org/10.1016/j.quageo.2013.08.003
Mathews WH, McTaggart KC (1969) Hope rockslide, British Columbia, Canada. In: Voight B (ed) Rockslides and avalanches natural phenomena. Elsevier, Amsterdam, pp 253–257
McColl S (2015) Landslide causes and triggers. In: Shroder J, Davies T (eds) Landslide hazards. Risks and Disasters. Elsevier, Amsterdam, pp 17–42
McColl ST, Davies TRH, McSaveney MJ (2010) Glacier retreat and rock-slope stability: debunking debuttressing. In: William AL et al (eds) Geologically active. Taylor and Francis, London, pp 467–474
McDougall S (2006) A continuum dynamic model for the analysis of extremely rapid landslide motion across complex 3D terrain. PhD Thesis, University of British Columbia
McDougall S, Hungr O (2004) A model for the analysis of rapid landslide motion across three-dimensional terrain. Can Geotech J 41(6):1084–1097. https://doi.org/10.1139/t04-052
McSaveney MJ, Davies TR (2006) Rapid rock mass flow with dynamic fragmentation: inferences from morphology and internal structure of rockslides and rock avalanches. In: Evans SG et al (eds) Landslides from massive rock slope failure. Springer, Dordrecht, pp 285–304
Moore JR, Gischig V, Katterbach M, Loew S (2011) Air circulation in deep fractures and the temperature field of an alpine rock slope. Earth Surf Process Landf 36:1985–1996. https://doi.org/10.1002/esp.2217
Moore JR, Gischig V, Amann F, Hunziker M, Burjanek J (2012) Earthquake-triggered rock slope failures: damage and site effects. In: Proceedings 11th International & 2nd North American Symposium on Landslides. CRC Press, Banff, pp 869–875
Nicolussi K, Kaufmann M, Patzelt G, van der Plicht J, Thurner A (2005) Holocene tree-line variability in the Kauner Valley, Central Eastern Alps, indicated by dendrochronological analysis of living trees and subfossil logs. Veget Hist Archaeobot 14:221–234. https://doi.org/10.1007/s00334-005-0013-y

Nicolussi K, Spötl C, Thurner A, Reimer PJ (2015) Precise radiocarbon dating of the giant Köfels landslide (Eastern Alps, Austria). Geomorphology 243:87–91. https://doi.org/10.1016/j.geomorph.2015.05.001
Nussbaum F (1934) Ueber die Formen von Bergsturzmassen, mit besonderer Berücksichtigung des Bergsturzes im Kandertal. Der Schweizer Geograph 11:12–13
Orwin JF, Clague JC, Gerath RF (2004) The Cheam rock avalanche, Fraser Valley, British Columbia, Canada. Landslides 4:289–298. https://doi.org/10.1007/s10346-004-0036-y
Ostermann M, Sanders D, Ivy-Ochs S, Alfimov V, Rockenschaub M, Römer A (2012) Early Holocene (8.6 ka) rock avalanche deposits, Obernberg valley (Eastern Alps): landform interpretation and kinematics of rapid mass movement. Geomorphology 171-172:83–93. https://doi.org/10.1016/j.geomorph 2012.05.006
Paguican EM, de Vries BV, Lagmay AM (2014) Hummocks: how they form and how they evolve in rockslide-debris avalanches. Landslides 11:67–80. https://doi.org/10.1007/s10346-012-0368-y
Pánek T, Hradecký J, Šilhán K, Smolková V, Altová V (2009) Time constraints for the evolution of a large slope collapse in karstified mountainous terrain of the south-western Crimean Mountains, Ukraine. Geomorphology 108:171–181. https://doi.org/10.1016/j.geomorph.2009.01.003
Parise M (2008) Rock failures in karst. In: Cheng Z et al (eds) Landslides and engineered slopes. CRC Press, Boca Raton, pp 275–280
Pesendorfer M, Loew S (2004) Hydrogeologic exploration during excavation of the Lötschberg base tunnel (AlpTransit Switzerland). In: Azzam R (ed) Engineering geology for infrastructure planning in Europe. Springer, Berlin, Heidelberg, pp 347–358
Pfiffner A (2010) The Helvetic nappe system and landscape evolution of the Kander valley. Schweiz Bull Angew Geol 15:53–61
Phillips M, Wolter A, Lüthi R, Amann F, Kenner R, Bühler Y (2017) Rock slope failure in a recently deglaciated permafrost rock wall at Piz Kesch (Eastern Swiss Alps), February 2014. Earth Surf Process Landf 42:426–438. https://doi.org/10.1002/esp.3992
Prager C, Zangerl C, Patzelt G, Brandner R (2008) Age distribution of fossil landslides in the Tyrol (Austria) and its surrounding areas. Nat Hazards Earth Syst Sci 8:377–407
Ravanel L, Deline P (2010) Climate influence on rockfalls in high-alpine steep rock walls: the north side of the Aiguilles de Chamonix (Mont Blanc massif) since the end of the Little Ice Age. The Holocene 21:357–365. https://doi.org/10.1177/0959683610374887
Santo A, Del Prete S, Di Crescenzo G, Rotella M (2007) Karst processes and slope instability: some investigations in the carbonate Apennine of Campania (southern Italy). Geol Soc Lond Spec Pub 279:59–72. https://doi.org/10.1144/SP279.6
Schleier M, Hermanns RL, Gosse JC, Oppikofer T, Rohn J, Tønnesen JF (2017) Subaqueous rock-avalanche deposits exposed by post-glacial isostatic rebound, Innfjorddalen, Western Norway. Geomorphology 289:117–133. https://doi.org/10.1016/j.geomorph.2016.08.024
Schulz WH, McKenna JP, Kibler JD, Biavati G (2009) Relations between hydrology and velocity of a continuously moving landslide—evidence of pore-pressure feedback regulating landslide motion? Landslides 6:181–190. https://doi.org/10.1007/s10346-009-0157-4
Shea T, de Vries BVW (2008) Structural analysis and analogue modeling of the kinematics and dynamics of rockslide avalanches. Geosphere 4:657–686. https://doi.org/10.1130/GES00131.1
Shugar DH, Clague JJ (2011) The sedimentology and geomorphology of rock avalanche deposits on glaciers. Sedimentology 58:1762–1783. https://doi.org/10.1111/j.1365-3091.2011.01238.x
Sosio R, Crosta GB, Hungr O (2008) Complete dynamic modeling calibration for the Thurwieser rock avalanche (Italian Central Alps). Eng Geol 100:11–26. https://doi.org/10.1016/j.enggeo.2008.02.012
Spreafico MC, Wolter A, Picotti V, Borgatti L, Mangeney A, Ghirotti M (2018) Forensic investigations of the Cima Salti Landslide, northern Italy, using runout simulations. Geomorphology 318:172–186. https://doi.org/10.1016/j.geomorph.2018.04.013
Stead D, Wolter A (2015) A critical review of rock slope failure mechanisms: the importance of structural geology. J Struct Geol 74:1–23. https://doi.org/10.1016/j.jsg.2015.02.002
Stone JOH, Allan GL, Fifield LK, Cresswell RG (1996) Cosmogenic chlorine-36 from calcium spallation. Geochim Cosmochim Acta 60:679–692. https://doi.org/10.1016/0016-7037(95)00429-7
Strom A (2006) Morphology and internal structure of rockslides and rock avalanches: grounds and constraints for their modelling. In: Evans SG et al (eds) Landslides from massive rock slope failure. Springer, Dordrecht, pp 305–326
Tinner W, Kaltenrieder P, Soom M, Zwahlen P, Schmidhalter M, Boschetti A, Schlüchter C (2005) Der nacheiszeitliche Bergsturz im Kandertal (Schweiz): Alter und Auswirkungen auf die damalige Umwelt. Swiss J Geosci 98:83–95. https://doi.org/10.1007/s00015-005-1147-8
Turnau V (1906) Beiträge zur Geologie der Berner Alpen. Wyss, Bern
Vockenhuber C, Miltenberger KU, Synal HA (2019) ^{36}Cl measurements with a gas-filled magnet at 6 MV. Nucl Instrum Meth B 455:190–194. https://doi.org/10.1016/j.nimb.2018.12.046
Walter F, Amann F, Kos A, Kenner R, Phillips M, de Preux A, Huss M, Tognacca C, Clinton J, Diehl T, Bonanomi Y (2020) Direct observations of a three million cubic meter rock-slope collapse with almost immediate initiation of ensuing debris flows. Geomorphology 351. https://doi.org/10.1016/j.geomorph.2019.106933
Wang YF, Cheng QG, Lin QW, Li K, Yang HF (2018) Insights into the kinematics and dynamics of the Luanshibao rock avalanche (Tibetan plateau, China) based on its complex surface landforms. Geomorphology 317:170–183. https://doi.org/10.1016/j.geomorph.2018.05.025
Weidinger JT, Korup O, Munack H, Altenberger U, Dunning SA, Tippelt G, Lottermoser W (2014) Giant rockslides from the inside. Earth Planet Sci Lett 389:62–73. https://doi.org/10.1016/j.epsl.2013.12.017
Wildberger A, Preiswerk C (1997) Karst und Höhlen der Schweiz/Karst et grottes de Suisse/Carso e grotte della Svizzera/Karst and Caves of Switzerland. Speleo Projects, Basel
Wolter A, Gischig V, Stead D, Clague JJ (2016) Investigation of geomorphic and seismic effects on the 1959 Madison Canyon, Montana, landslide using an integrated field, engineering geomorphology mapping, and numerical modelling approach. Rock Mech Rock Eng 49:2479–2501. https://doi.org/10.1007/s00603-015-0889-5
Yin Y, Sun P, Zhang M, Li B (2011) Mechanism on apparent dip sliding of oblique inclined bedding rockslide at Jiweishan, Chongqing, China. Landslides 8:49–65. https://doi.org/10.1007/s10346-010-0237-5
Zerathe S, Lebourg T, Braucher R, Bourlès DL (2014) Mid-Holocene cluster of large-scale landslides revealed in the Southwestern Alps by ^{36}Cl dating. Insight on an Alpine-scale landslide activity. Quat Sci Rev 90:106–127. https://doi.org/10.1016/j.quascirev.2014.02.015
Ziegler HJ, Isler A (2013) Lötschberg Basistunnel: Zusammenfassender geologischer Schlussbericht. Berichte der Landesgeologie 4. Swisstopo, Wabern
Zwahlen P (1986) Die Kandertal-Störung: eine transversale Diskontinuität im Bau der Helvetischen Decken. Dissertation, Universität Bern

Electronic supplementary material The online version of this article (https://doi.org/10.1007/s10346-020-01365-y) contains supplementary material, which is available to authorized users.

C. Singeisen · S. Ivy-Ochs (✉) · A. Wolter
Department of Earth Sciences,
ETH Zurich,
8092, Zurich, Switzerland
Email: ivy@phys.ethz.ch

S. Ivy-Ochs · O. Steinemann · C. Vockenhuber
Laboratory of Ion Beam Physics,
ETH Zurich,
8093, Zurich, Switzerland

N. Akçar · S. Yesilyurt
Institute of Geological Sciences,
University of Bern,
3012, Bern, Switzerland